Review

Elektrotech. Inftech. (2025) 142:312–345
https://doi.org/10.1007/s00502-025-01331-3



e+i elektrotechnik und informationstechnik

# Advances in electric motors: a review and benchmarking of product design and manufacturing technologies

**David Drexler · Achim Kampker · Henrik Born · Michael Nankemann · Sebastian Hartmann · Tobias Kulawik**

Received: 9 May 2025 / Accepted: 10 June 2025 / Published online: 15 July 2025
© The Author(s) 2025

**Abstract** Electric drive units are key components of the drivetrain of electric vehicles. In recent years, the product topology of the motor and the respective components as well as the underlying manufacturing technology have changed fundamentally against the background of different design objectives of the manufacturers and are also subject to a high degree of variance. To identify significant development trends in this dynamic sector and to contribute to further optimization of electric drives, traction drives of electric vehicles from the recent years are analyzed and compared regarding their characteristics. To achieve this goal, a systematic analysis and categorization of 31 electric vehicles from 2018 to 2023 and 48 electric traction motors installed in them is carried out. The investigation is conducted using a top-down analysis, starting with a macroscopic view of the motor down to microscopic analysis of individual components at stator and rotor level. Macroscopic analysis considers the overall structure of the electric motor and power electronics, while microscopic analysis takes a detailed look at the product design and the production technology used.

**Keywords** Electric motor design · Product technology · Process technology · Technical benchmarking study

D. Drexler (✉) · A. Kampker · H. Born · M. Nankemann · S. Hartmann · T. Kulawik
Chair of Production Engineering of E-Mobility Components, RWTH Aachen University, Aachen, Germany
d.drexler@pem.rwth-aachen.de

## Technologischer Fortschritt bei Elektromotoren: eine Vergleichsstudie von Produktdesign- und Fertigungstechnologien

**Zusammenfassung** Elektrische Antriebseinheiten stellen eine Schlüsselkomponente des Antriebsstrangs von Elektrofahrzeugen dar. In den letzten Jahren haben sich die Produkttopologie des Motors und der jeweiligen Komponenten sowie die zugrunde liegende Fertigungstechnologie vor dem Hintergrund unterschiedlicher Konstruktionsziele der Hersteller grundlegend verändert. Entsprechend groß ist die Varianz. Um wesentliche Entwicklungstrends in diesem dynamischen Umfeld zu identifizieren und einen Beitrag zur weiteren Optimierung elektrischer Antriebe zu leisten, werden in dieser Arbeit Traktionsantriebe von Elektrofahrzeugen der letzten Jahre hinsichtlich ihrer Eigenschaften analysiert und verglichen. Zu diesem Zweck werden 31 Elektrofahrzeuge aus den Jahren 2018 bis 2023 und die darin verbauten 48 elektrischen Traktionsmotoren einer systematischen Analyse und Kategorisierung unterzogen. Die Untersuchung erfolgt anhand einer Top-Down-Analyse, die mit einer makroskopischen Betrachtung des Motors beginnt und mit einer mikroskopischen Analyse einzelner Komponenten auf Stator- und Rotorebene endet. Während die makroskopische Analyse die Gesamtstruktur des Elektromotors und der Leistungselektronik betrachtet, wirft die mikroskopische Analyse einen detaillierten Blick auf das Produktdesign und die verwendete Fertigungstechnologie.

**Schlüsselwörter** Gestaltung von Elektromotoren · Produkttechnologie · Fertigungstechnologie · Technische Vergleichsstudie

## 1 Introduction

For the automotive sector, the battery-electric powertrain concept represents a suitable solution for decarbonized mobility and is therefore a key factor in achieving climate targets [1, 2]. Regarding the substitution of the conventional combustion engine with an electrified powertrain, innovative manufacturing and product technologies are a decisive factor for an increased vehicle range, reduced production costs as well as sustainable and long-lasting product life cycles.

This applies in particular to the electric traction motor, for which a continuous optimization of the prevailing product designs on the market can be identified [3]. The optimization is driven by the target of producing a cost-optimized, efficient, compact and light and powerful electric drive unit [4, 5]. The different design objectives as well as the continuous optimization have led to a wide variety of product and production technologies in the field of electric traction motors.

Reviewing and analyzing the variety of products on the market and the respective manufacturing technologies used to produce the motors is a crucial step in identifying development trends in this sector, improving electric motors currently available and thus contributing to establishing the electric drivetrain in vehicles [6].

## 2 State of the literature

In the literature, a number of approaches can be identified in which the different product technologies related to electric motors are examined and analyzed using benchmarking studies.

El Hadraoui et al. [7] and Oktav [8] categorize the different types of motors used in automotive applications in terms of performance, reliability and efficiency. However, both do not examine the individual components, the specific design and their technological development in more detail.

A comprehensive overview of the latest studies and analyzes on cooling technologies and calculation methods for traction motors in electric vehicles can be found in the work of Wrobel [9] and Gai et al. [10], which present various cooling concepts, such as active jacket cooling. In addition, individual concepts from electric vehicles are compared and evaluated in a real setup. In their research Krings et al. [11] have focused on permanent magnet traction motors for electric and hybrid vehicles. In particular, the electromagnetic motor design and the arrangement of the permanent magnets in relation to the performance characteristics of the respective motors are analyzed for ten vehicles from the years 2010 to 2019.

Agamloh et al. [4] analyzed the technological development status and the product technology trends of traction motors for electric vehicles. The focus is on Permanent Magnet Synchronous Motors (PMSMs), rare earth magnet-free traction motors and the development of the thermal management system. Overall, in Agamloh et al. the motor design and performance data of 18 motors from 2006 to 2017 is analyzed without taking a closer look at the specific design of the motor components.

In addition to analyzing the cooling methods and performance data, a specific investigation including a few individual motor components is carried out in the work of Husain et al. [3]. Using selected benchmarking data sets with a small sample size of vehicle models from 2004 to 2020, an evaluation of the technology and specific product characteristics like the copper mass or the magnetic mass is performed to derive trends.

## 3 Research deficit and motivation

Following an in-depth review of the available literature, four key areas for improvement have been identified. Firstly, the available literature lacks relevance in terms of timeliness, with insufficient analysis of vehicles from recent years. This is a significant issue, given the rapid shift from conventional to electric drives [12] as well as the huge advancement in the electric motor technology [13, 14]. Furthermore, the analysis is often limited to a high-level overview, with insufficient attention paid to the individual components. When a more detailed examination is conducted, it is frequently done in isolation, without considering the interactions between components or the overall system. Further, the sample size of the available studies is limited, which lowers the significance of the findings. Lastly, most of the studies are limited to the product technologies of the electric motor and an in-depth analysis of current electric motors on the market regarding the process technology used for the components of the motor does not take place.

To address these downsides of the available literature, a comprehensive analysis of electric motors based on available electric vehicles will be carried out in this paper focusing onto the underlying product and process technology. To be able to analyze technological trends, older vehicle models and their drive units will be included in addition. The technical data presented in this study originate from the A2MAC1 [15] as well as the ADAC database [16] and were supplemented by tear-down studies conducted at the PEM of the RWTH [17] and a comprehensive literature search.

## 4 Classification of the sample and evaluation approach

The sample size of the product and process-related properties of electric drive motors analyzed in this study comprises 48 motors from a total of 31 vehicles from different manufacturers from the years 2018

to 2023 (see Appendix Table 1.). The table provides an overview of the manufacturer, the specific model name, the date of market entry of the model, the position of the engine in the vehicle, the engine topology and the associated performance data with a distinction between continuous and peak power. The continuous and peak power outputs listed in the table are all taken from the ADAC vehicle database [16]. The factor, which is shown in the last column, is calculated from the quotients of continuous and peak power.

30 of these motors are PMSMs and nine are Induction Motors (IM) and nine are Externally Excited Eynchronous Machines (EESMs), representing a percentage share of 62.5% and 18.75% respectively. Most of the vehicles analyzed use an all-wheel drive configuration, while the second most vehicles feature a front-wheel drive. Based on the categorization of motor vehicles according to the European commission [18], most of the vehicles considered are mid-range and luxury cars (Class C and D). Although small cars (Class A and B) as well as luxury vehicles (Class E and F) are included in the study, they play a comparatively minor role in terms of quantity.

The analysis is carried out according to a top-down approach, initially at the macroscopic level of the drive unit, consisting of the motor and the associated reduction gearbox. The macroscopic analysis includes an examination of the arrangement and structure of the motor housing, the gearbox and the power electronics. Subsequently, an evaluation of the motor performance is carried out in relation to the weight of the motor and corresponding gearbox. Finally, a brief analysis of the general powertrain concept is provided.

In a subsequent microscopic view, the components of the respective motors and the interface between them are considered and analyzed regarding the product and manufacturing technologies in detail. The investigation is first carried out for all components of the stator and then the rotor. Finally, the interface between those two assemblies is analyzed. In this context, the dimensions and weight of the components are also discussed in addition to the manufacturing and product technology. Also a link to performance data is established at the appropriate point. In general, if specific information is not available or cannot be determined, the respective vehicle is excluded for this specific component evaluation but remains included in all other evaluations for which the information is available. To ensure transparency, the sample size $n$ included in the evaluation is therefore also indicated.

To get the best possible overview of the characteristics of certain design parameters for all motors in the sample, the evaluation is conducted primarily with the help of boxplots. To make it easier to interpret the displayed data, this will initially be explained using an example (see Fig. 1). The central box, which is bounded by the Quartiles 1 and 3, indicates the range, also known as the interquartile range, in which the middle 50% of the data lie. The solid line within the box describes the mean value and the cross indicates the position of the mean value. The T-shaped whiskers (maximum (Max) and minimum (Min) without outliers) extend to the last data point that is still within 1.5 times the interquartile range. If data points are further away, they are referred to as outliers and marked with a small circle in the scale [19]. In addition, the sample size, the average value, the deviation within the sample, and the maximum and minimum values in the sample are documented and used for analysis to classify the sample and the parameter values.

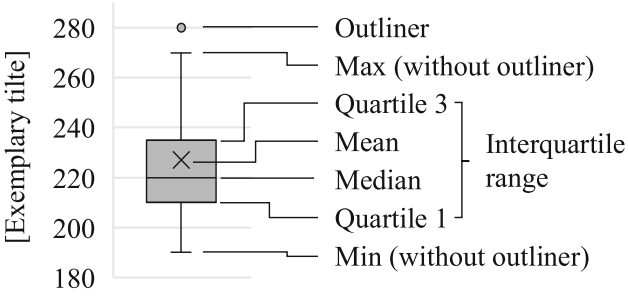



Fig. 1 Generic representation of a box plot for visualizing the evaluation of samples. $n$ Sample size, ∅ Average within sample, $\sigma$ Standard deviation in sample, *Max* Maximum, *Min* Minimum

## 5 Analysis of product and process technology study

### 5.1 Macroscopic observation of the drive unit

#### 5.1.1 Motor housing, gearbox and power electronics arrangements and structure

Within the 48 analyzed electric motors, a wide variety of structures and arrangements of gearboxes, motor housings and power electronics can be identified, which differ regarding the degree of integration of the three components. A top view of the identified structures is shown in Fig. 2. In some designs and arrangements of gearboxes, motor housings and power electronics, the individual components have different details. In cases a), b), e) and h), for example, there are two different possible shapes for the bearing shields or the additional housing element, which are designated Bearing Shield Configuration 1 (BSC 1) and 2 (BSC 2) or Additional Housing Element Configuration 1 (AHEC 1) and 2 (AHEC 2). In actual application, one of these two configurations is implemented (see Fig. 2a,b,e,h). The additional housing cannot be directly assigned to the gearbox or motor and act as connecting elements between the structures (see Fig. 2f,g,h).

The motor housing, marked with a hatch pattern running from left to right, is usually a cast aluminium or extruded profile that is open on both sides or on

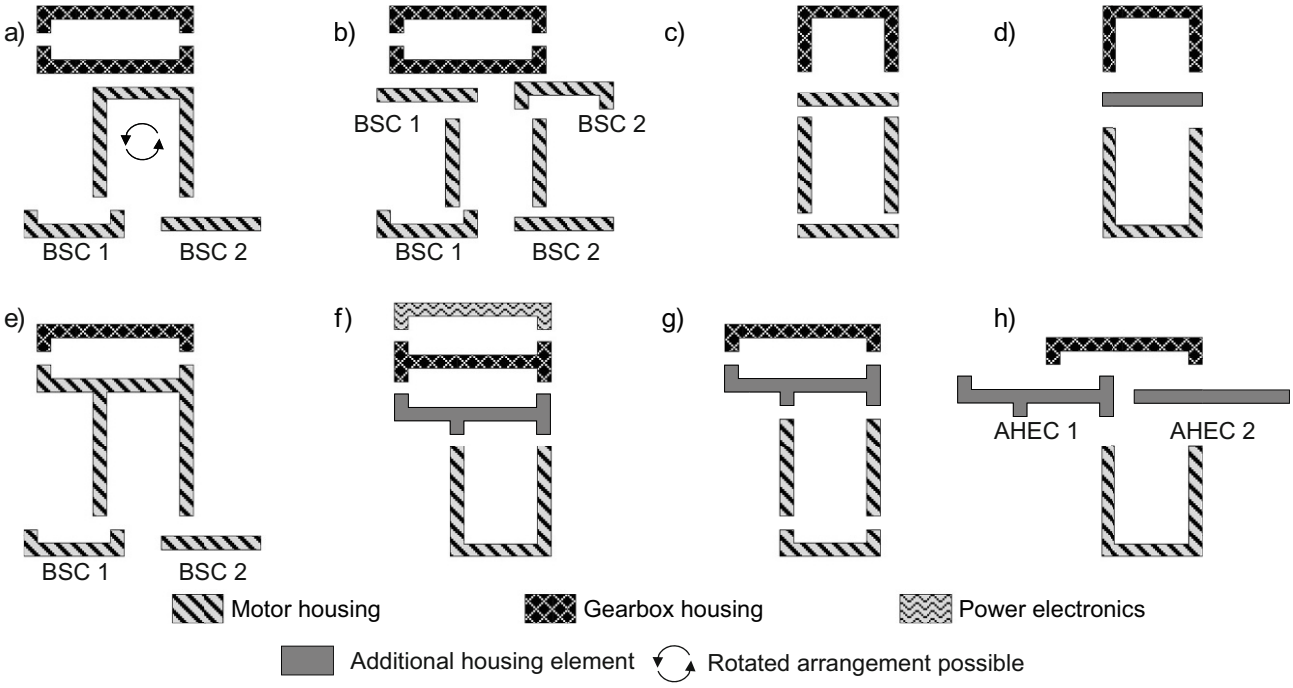



Fig. 2 Overview of identifying arrangements and structures of motor, gearbox and power electronics in top view. *BSC 1* Bearing shield configuration 1, *BSC 2* Bearing shield configuration 2, *AHEC 1* Additional housing element configuration 1, *AHEC 2* Additional housing element configuration 2

one side and closed on both sides or on one side by a bearing shield (see Fig. 2a to h). The bearing shield can be flat or shell-shaped (see Fig. 2a,b,e).

The reduction gear is usually housed in two shell-shaped elements (see Fig. 2a,b,e,f,g,h) or a hat-shaped element which is closed by a flat structure (see Fig. 2c, d). The shell-shaped structure and the hat profile are also usually designed as cast components. In most cases, the reduction gear is flanged to the side of the motor housing, so that the output shaft of the gear, from which the torque is transmitted to the two wheels of a drive axle, is parallel to the motor axis. Accessibility from the gear output to the two output wheels is easily provided by the parallel offset of the output axis and the motor axis. Examples of this drive unit structure are all electric motors of the BMW Gen 5 generation as well as the front and rear motor of the BYD Seal Excellence and Tang EV.

The variants in Fig. 2c and d represent an alternative to this arrangement and design of the motor and gearbox housing. Although the gearbox is also flanged to the side, the gearbox axis is coaxial with the motor axis. In both cases, the gearbox housing is a simple hat structure that is closed off by a flat structure. The motor housing itself is either also formed by a hat profile that is closed off by an additional element or is designed as a hollow cylinder that is closed off on both sides by a flat structure. In both configurations, the hat profile of the gearbox and the motor share a structure at the end. Examples of this structure are both motors of the Jaguar I-Pace and the front and rear motors of the Polestar 2 from 2020 and 2023.

In most cases, the power electronics are located on top of the motor or gearbox housing and are therefore not shown in top view section cut (see Fig. 2a,b,c,d,e,g,h). The power electronics can be easily mounted and screwed onto the motor housing and gearbox as a separate component. Alternatively, the motor housing can have a recess on the top that forms both the top of the motor housing and the bottom of the power electronics housing. This is implemented, for example, in the BMW Gen 5 housing and in both motors of the NIO ET 5 Long Range. The integration of the housing structures results in a reduction in the number of components required, the number of additional elements for connecting separate structures, the assembly processes and the number of mechanical interfaces [20]. On the other hand, however, there is greater complexity in terms of manufacturing the housings.

An exception is the structure shown in Fig. 2f, in which the power electronics is flanged to the side of the gearbox. In this case, the phase ends of the electric motor are longer and extend through the transmission housing to the power electronics. The structure is implemented in all motors of the two Tesla Model Y models.

About 50% of the examined drive units have a structure corresponding to the schematic drawing in Fig. 2e. This finding confirms the general trend towards integrated drive systems [21]. Drive units composed of a large number of individual components, as shown in Fig. 2b, are no longer found in newer vehicles and can only be identified in vehicles

such as the Nissan Leaf Tekna and the Peugeot 208 e GT.

#### 5.1.2 Power-to-weight ratio for continuous and peak power

Based on the analysis of a vehicles, it can be concluded that vehicles with an All-Wheel Drive (AWD) configuration primarily belong to vehicle classes C to F, while vehicles with only one drive, i.e. Rear-Wheel Drive (RWD) or Front-Wheel Drive (FWD), belong to classes A to D (see Appendix Table 1). This observation can be attributed to the fact that a higher vehicle class generally also means a higher unladen weight. This in turn requires higher performance for the powertrain.

A closer look at the performance of the vehicles in the sample reveals that in terms of peak power, which can be called up for short periods, the PMSM of the Tesla Model Y RWD with 235 kW and the front motor of the Mercedes EQS 580 4Matic AMG Line with 245 kW have the highest power output (see Fig. 3). The EESM of the BMW iX xDrive 50 and the BMW i7 xDrive60 have slightly lower peak power outputs of 230 kW. The peak power of the IM is generally lower, at 158 kW for the front motor of the Tesla Model Y AWD Standard Range and 165 kW for the rear motor of the Audi e-tron 55 Quattro Edition One, for example.

When looking at the continuous power of the motor, the differences between the motor topologies PMSM, IM and EESM can also be detected (see Fig. 4). The continuous power of PMSM is significantly higher than that of EESM. The rear motor of the Polestar 2 Long Range Dual Motor (2023) has the highest continuous power with 133 kW, followed by 109 kW of the IM of the Mercedes EQS 580 4MATIC.

In addition to absolute power, PMSMs also outperform IM and EESM in terms of power density, whereby the mass is given by the motor and gearbox mass (see Fig. 5). The PMSMs with the highest peak power density are the rear motor of the NIO ET5 with 3.28 kW/kg and the rear motor of the Tesla Model Y RWD with 3.00 kW/kg. In contrast, the IM of the Tesla Model Y AWD Standard Range has a peak power density of 2.48 kW/kg, while the EESM of the Nissan Ariya Evolve has a peak power density of 2.25 kW/kg. Therefore, in terms of both continuous power and peak power, PMSMs continue to represent the motor topology with the highest power. However, it should be noted also that significant improvements have been made in the performance density of IM and ESSM in recent years. These become particularly clear when plotting the peak power density of all motors as a function of model year. For all three motor topologies, a clear linear trend line can be identified here, rising from left to right, although it is steeper for the IM and EESM than for the PMSM.

For the EESM the performance data for the Renault Megane E-Tech from 2022 and the Renault Zoe R135 from 2019 can be used as examples. The motor and transmission of the Renault Zoe R135 are approximately 20 kg heavier than those of the Renault Megane E-Tech. Despite its smaller and more compact motor, the Megan E-Tech delivers a higher continuous power with 55 kW and a peak power that is 60 kW higher and amounts to 160 kW. In this particular case, the power density was increased from 1.02 kW/kg to 2.02 kW/kg.

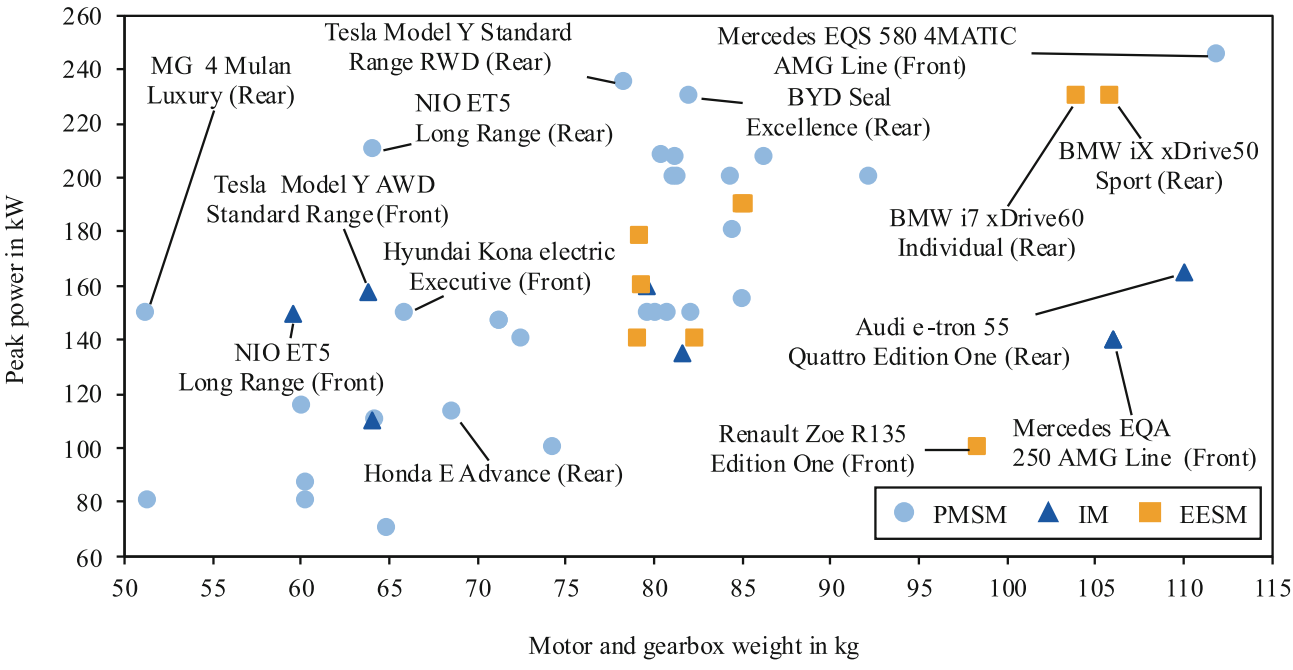



Fig. 3 Peak power of the motors plotted against the weight of the motor and gearbox depending on the motor topology, *PMSM* Permanent magnet synchronous motor, *IM* Induction machine, *EESM* Externally excited synchronous machines

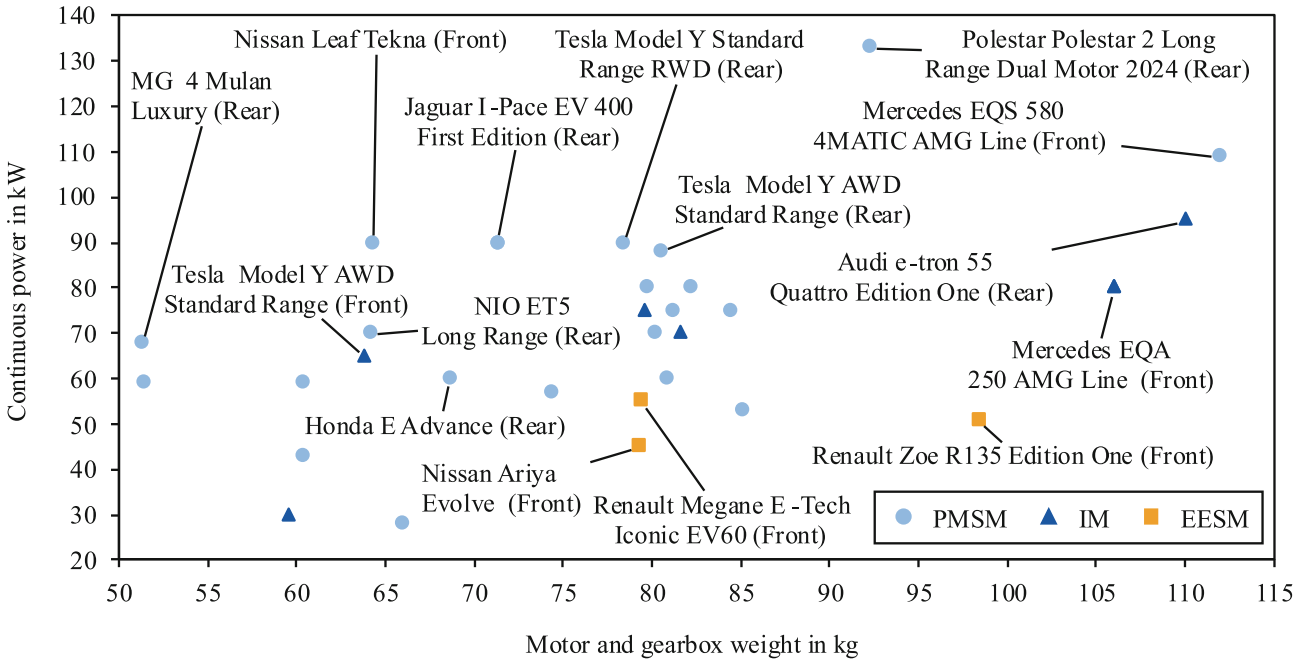



Fig. 4 Continuous power of the motors plotted against the weight of the motor and gearbox depending on the motor topology. *PMSM* Permanent magnet synchronous motor, *IM* Induction machine, *EESM* Externally excited synchronous machines

Accordingly, numerous innovations have been made in the three years between these two models, leading to an increase in power density.

The same can be identified for the IM topology. The motor of the 2021 Mercedes EQA250, with a motor and transmission weight of 105.95 kg, generates a continuous output of 80 kW and a peak output of 140 kW. With a weight reduction of more than 25 kg, the front motor of the BYD Seal Excellence from 2023 achieves comparable performance values with 75 kW continuous power and 160 kW peak power. The power density increased from 1.32 kW/kg to 2.01 kW/kg.

As described, there is a significant increase in power density for PMSMs as well. However, the power density of this motor topology was already at a high level in 2018, for example with the front and rear motor of the Jaguar I-Pace EV at 2.06 kW/kg and the front motor of the Hyundai Kona Electric Executive at 2.27 kW/kg. Despite this, the power density for the rear motor of the Nio ET5, for example, with 3.2 kW/kg, and the rear motor of the Tesla Model Y could be increased to over 3.0 kW/kg.

#### 5.1.3 Power-to-weight ratio for continuous and peak power

Based on the analysis of the continuous performance data (see Fig. 4), three drive concepts can be identified within the sample.

- *Single drive*: The vehicle is equipped with a front or rear motor. The motor is a PMSM or ESSM. Examples for this concept are the Hyundai Kona electric Executive (FWD) or Nissan Leaf Tekna (RWD) from 2018.
- *Dual drive with similar performance*: In this drive configuration, the vehicle has two different motors with similar power, as in the Audi e-tron 55 Quattro Edition One from 2019, or two identical motors with the same power, as in the Jaguar I-Pace, Toyota bZ4X, the Polestar 2 Long Range Dual Motor (2020) the BMW iX1 xDrive30 Premium or the Fisker Ocean One 2023. The same motor topology is generally used for the front and rear motors (IM-IM, EESM-EESM and PMSM-PMSM). The variant with two identical motors offers the advantage of common parts, which reduces manufacturing costs.
- *Main drive and additional auxiliary drive*: In this configuration, a PMSM is combined with an IM or PMSM as the auxiliary drive. The auxiliary drive usually has a reduced continuous power but high peak power, as in the case of the NIO ET5 Long Range (AWD), for example, or for use at low continuous loads or to absorb peaks. According to the analysis of the NIO ET5 Long Range, Polestar 2 Long Range Dual Motor, BYD Seal Excellence and Tesla Model Y AWD Standard Range vehicles, the PMSM is usually installed in the rear and the IM in the front of the vehicle.

These three configurations result in different requirement profiles for the design of PMSM, IM and EESM regarding the speed-torque characteristic map.

### 5.2 Microscopic observation of the components

The following section provides a more detailed look at the design of the rotor and stator and their interfaces.

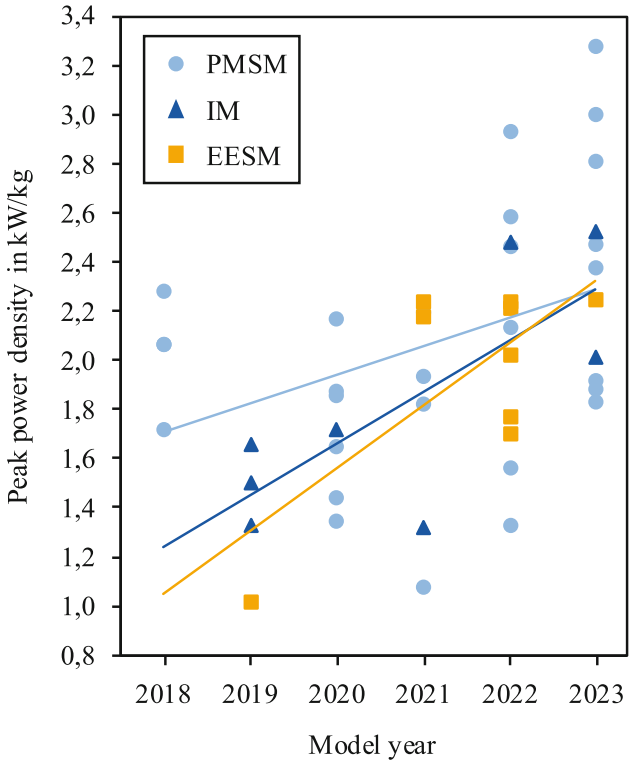



Fig. 5 Peak power density for motors from the sample depending on motor topology. *PMSM* Permanent magnet synchronous motor, *IM* Induction machine, *EESM* Externally excited synchronous machines

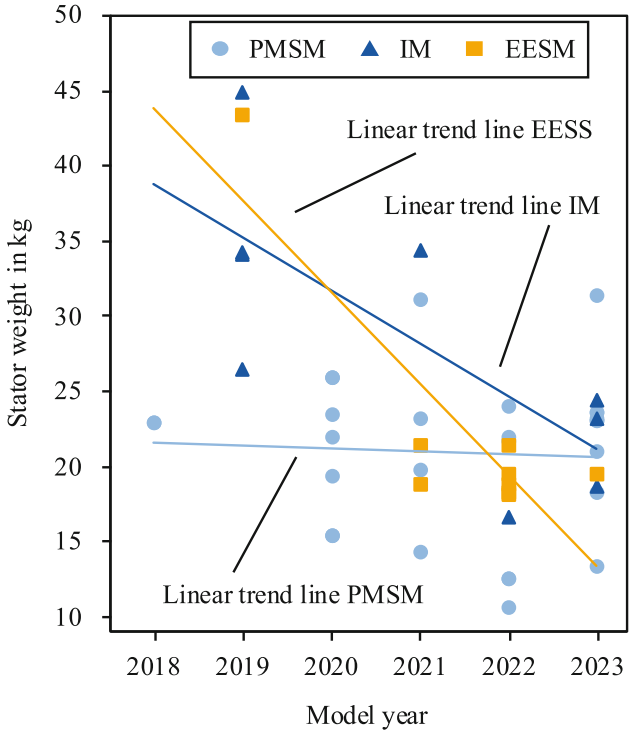



Fig. 6 Stator weight for motors from the sample depending on motor topology. *PMSM* Permanent magnet synchronous motor, *IM* Induction machine, *EESM* Externally excited synchronous machines

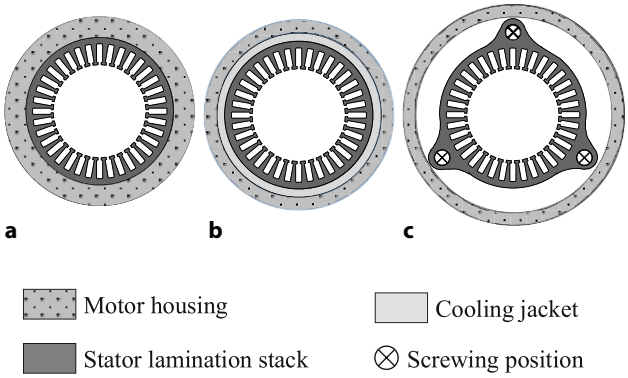



Fig. 7 Schematic representation of the identified concepts for the interface between the motor housing and the stator

### 5.2.1 Stator

The stator consists of numerous individual components. Since many of these components account for a significant proportion of the total weight of the drive unit due to the used materials, the development of the total weight of the stator will be discussed before the individual design features and structures of the stator components are examined.

The previously mentioned significant increase in power-to-weight ratios for IM and EESM can be partly explained by the stator weight data for the model year. (see Fig. 6).

The trend line for both motor topologies clearly shows that the stator weight for these two motor topologies has been significantly reduced over the period under consideration. Compared to the significant reduction in stator weight for IM and EESM, the stator weight for PMSM only decreases slightly between 2018 and 2023 and further shows a high degree of variation. Examples here are the stator of the rear motor of the Polestar 2 Long Range Dual Motor (2023) with 31.32 kg and the rear motor of the MG 4 Mulan Luxury from 2022 with 10.61 kg.

**Interface between stator and stator housing** The stator of the electric motor is surrounded by a housing element to protect it from external environmental influences and to secure it to the vehicle chassis. Two different concepts can be identified regarding the method of fixing the stator in the housing and the design of the interface.

The first concept involves fastening the stator directly in the housing or in a separate cooling jacket by means of a force-fit connection (see Fig. 7a,b). The force fit is created by a shrink fit or press fit connection. In the shrink fit connection, the housing or cooling jacket is heated inductively or conductively and expands. The stator is inserted into the expanded structure. A subsequent cooling process of the housing or the cooling jacket causes it to contract and fix the stator in place. In case of a press fit, the stator is pressed directly into the cooling jacket or the housing by means of pressing force. If a separate cooling

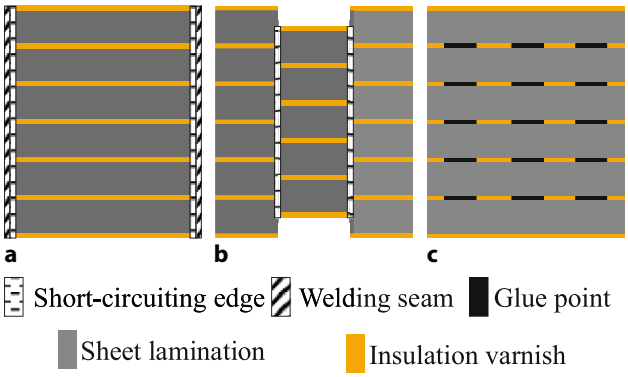



Fig. 8 Schematic representation of the three identified stator sheet lamination stack packaging technologies: Welding (**a**), interlocking (**b**) and glueing (**c**)

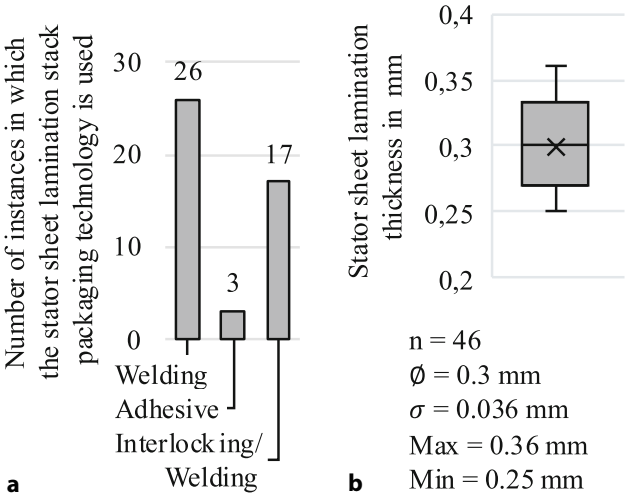



Fig. 9 Evaluation of the distribution of different stator sheet lamination packaging technologies (**a**) and of the stator sheet lamination thickness (**b**). *n* Sample size, ∅ Average within sample, $\sigma$ Standard deviation in sample, *Max* Maximum, *Min* Minimum

jacket is used, it is usually fixed to the motor housing in combination with the pressed-in stator using a screw connection.

Instead of shrinking or pressing, the stator can also be fixated by mechanically screwing the stator sheet lamination stack into the housing. For this purpose, the stator sheet lamination stack is provided with corresponding holes in the yoke through which it can be screwed to the housing (see Fig. 7c). In this case, there is a gap between the housing and the stator to allow easy assembly of the stator sheet lamination stack into the housing.

Approximately 81.25% of the motors examined are fixed in the housing using shrink/press fit connections. Examples are all models from Mercedes, BMW, Polestar, Tesla, VW, Audi, Volvo and Jaguar. The remaining 18.75% of the examined motors, mostly models from Asian manufacturers like Hyundai, Toyota, BYD and Nissan, are fixed in the housing using a screw connection.

**Stator sheet lamination stack** The stator sheet lamination stack is responsible for guiding and amplifying the magnetic field and consists of thin individually insulated ferromagnetic sheets [22]. To facilitate the stacking process, the sheet laminations are often stacked to segments with a specific height. Afterwards several of these segments are joined together to form a complete stator sheet lamination stack. Within the analyzed samples, the number of segments varies between one and nine and shows no dependence on the year of manufacture or the height of the stator sheet. On average, the stator sheet lamination stacks consist of five segments. To achieve the necessary mechanical strength of the stator lamination stack, the individual sheet laminations must be connected to each other. For this, three different methods could be identified.

56.5% of the sheet lamination stacks are connected to each other using several welds on the outer radius of the sheet laminations stack in axial direction over the entire active length of the sheet lamination stack (see (Fig. 8a). If the stator is pressed or shrink-fitted into the housing or the cooling jacket, the weld is usually located within a recess in the sheet lamination stack. This is because the geometry of the weld seam is difficult to control and may cause collisions and damages when pressing in the stator. Welding for packaging is a cost-effective method, especially for high production volumes, and results in a high strength of the sheet metal stack [23]. These reasons cause that 26 of the examined 46 stator sheet lamination stacks use this packaging technology (see (Fig. 9a).

However, the weld seam on the outer radius forms a short-circuit edge, which has a negative effect on the electromagnetic properties of the stack and results in higher sheet metal stack losses during subsequent operation. The heat input into the sheet lamination stack during welding can also cause deformation [23, 24]. Further, the sheet laminations are only fixed to each other at the outer radius with no additional fixed in the stator teeth area, which reduces mechanical strength and promotes detachment in the area of the stator tooth.

Another packaging method is given by interlocking (see Fig. 8b). Hereby, a punching tool is used during the stacking process to deform the single sheet laminations in a small area in axial direction. The deformation ensures a form-fitting connection/clamping between the adjacent sheet lamination and thus a mechanical connection of the entire stack. The depth of the punching/deformation depends on the thickness of the sheet lamination and can be up to 80% of the sheet lamination thickness. Like welding, this process is inexpensive to implement and can be used in large quantities. However, the excess material resulting from the punching creates a contact surface between the sheet laminations, which leads to stronger

induction of eddy currents, resulting in increased iron losses during operation. Furthermore, it causes significantly lower mechanical stability, particularly compared to welded sheet lamination stacks [25]. This process is used in a total of 17 of the 46 examined stator sheet lamination stacks (see Fig. 9a). The stator sheet lamination stacks of the front motor of the Tesla Model Y AWD Standard Range are stamped in a segment. The segments are then welded together.

A rarely used alternative is bond packaging (see Fig. 8c). In this process, adhesive dots are applied to the sheets using fine nozzles before the sheets are punched. The adhesive dots are distributed across the whole sheet lamination, ensuring a large-area adhesion between the individual sheet laminations. Although this process is more cost-intensive than welding, it offers improved electrical properties, precision and tolerance accuracy [25]. The process is used in three newer motors namely the rear motor of the Tesla Model Y AWD Standard Range and the front and rear motors of the Hyundai Ioniq 5 Project 45 (see Fig. 9a).

One of the numerous design parameters relating to the stator sheet lamination stack is the thickness of each individual sheet laminations. The following evaluation is based on the total thickness of the sheet lamination, including the insulation layer on the top and bottom (see Fig. 9b). The average sheet lamination thickness of all motors evaluated is 0.3 mm. Regarding the evaluation of thickness over time, it can be seen that older models such as the front motor of the Audi e-tron 55 Quattro Edition One and the Aiways U5 Premium with a thickness of 0.35 mm or the Renault Zoe R135 Edition One with 0.36 mm used significantly thicker sheet laminations than newer models such as the Tesla Model Y RWD, Polestar 2 Long Range Dual Motor (2023) or the Toyota bZ4X with a sheet thickness of 0.25 mm.

The trend towards thinner sheet thicknesses can be referred to reduction in iron losses during operation using thinner sheet laminations. Accordingly, a low sheet lamination thickness results in increased efficiency and thus greater range of the vehicle [26]. The limitation of the sheet thickness lies in the processing, as sheets with lower sheet thickness are more difficult to process. It has been shown that reduced losses during operation justify higher production costs due to lower thickness.

The outer diameter of the stator sheet and thus of the stator is an important parameter for the required installation space. Due to the high cost of the stator sheet lamination stack, the diameter of the stack also plays a major role in the cost of the drive unit, and manufacturers are striving to reduce the amount of material used for the sheet lamination stack accordingly [22, 27].

Within the sample the outer diameter varies between a maximum of 280 mm and a minimum of 170 mm, with an average outer diameter of 222 mm (see Fig. 10a). Regarding the development of the outer diameter over the period under review from 2018 to 2023, a trend towards a reduction in diameter can be observed. While the motors from 2018 and 2019 have an average outer diameter of 244 mm, that of the motors from 2023 is 219 mm. For the predominant motor topologies EESM, IM and PMSM, significant differences can be observed in terms of outer diameter. The average outer diameter of IMs is 237.22 mm, which is significantly higher than that of EESM with 211 mm and PMSM with 219.27 mm. This may be because motor manufacturers are trying to compensate for the lower power density of IM compared to PMSM and EESM by using a larger motor diameter.

The outer diameter, in conjunction with the inner diameter, is a decisive parameter for the mass of the stator sheet lamination stack. The inner diameter, in combination with the air gap and the outer rotor diameter, determines the effective air gap diameter of the motor and is decisive for the torque of the motor and its performance characteristics. Therefore, it seems logical that based on the analyzed data, the trend towards reduced outer diameter cannot be transferred to the inner diameter and that the trend towards reduction is significantly less pronounced. For motors from 2018 and 2019 an average value of 151 mm and a value of 146 mm for motors from 2023 can be determined. The significantly smaller reduction in inner diameter compared to outer diameter is likely due to the important role of the inner diameter for motor torque [28–30].

On average, the examined electric motors have an internal diameter of 148.87 mm, with the smallest internal diameter of 117 mm found in the front motor of the Volvo EX30 Twin Motor and the largest motor

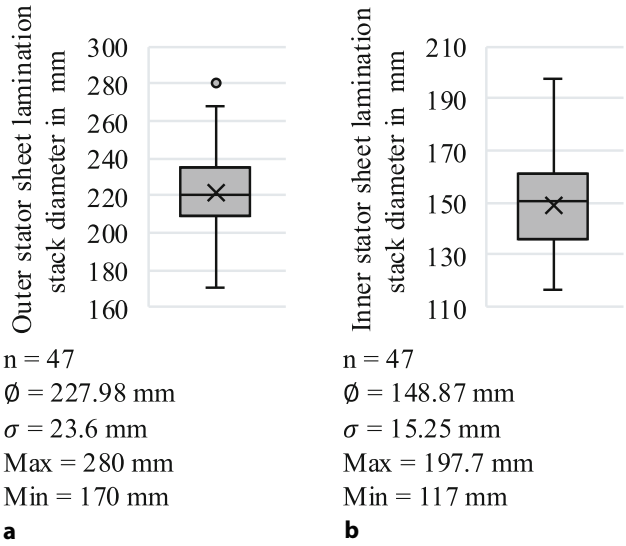



Fig. 10 Evaluation of the outer stator sheet lamination stack diameter (**a**) and of the inner stator sheet lamination stack diameter (**b**). *n* Sample size, ∅ Average within sample, $\sigma$ Standard deviation in sample, *Max* Maximum, *Min* Minimum

of just under 197.7 mm in the motor of the Honda Advanced E (see Fig. 10b).

Like the inner diameter, the length of the stator sheet lamination stack is a decisive parameter for the power and torque of the motor as well as its installation space [30, 31]. On average, the motors in the sample have an active length of 136.8 mm (see Fig. 11a). The stator with the longest active length of 202.4 mm is given by the front and rear EESM of the BMW iX1 xDrive30 Premium. The motor of the Honda Advanced E, which has the largest outer diameter, has the shortest active length with 62 mm. Over the period under review from 2018 to 2023, it can be observed that the active length has been reduced and the required axial installation space is correspondingly smaller. While motors from 2018 and 2019 have an average active length of 161 mm, this is significantly shorter for motors from 2023 with 130 mm.

A difference between the motor topologies can also be identified in terms of active length. On average, the active length of EESM is significantly higher than that of IM and PMSM. EESM have an average active length of 153.77 mm, while PMSM and IM are on average barely 20 mm shorter with 132.164 mm and 134.33 mm. This fact as well as the evaluation of the inner stator diameter leads to the assumption, that manufacturers are attempting to compensate for the lower power density of EESMs compared to PMSMs by a longer active length, while for IMs manufacturers attempt to do so with the rotor diameter or the effective air gap diameter.

Combining the trend towards shorter active lengths with the reduction in the outer diameter and the slight decrease in the inner diameter, it becomes apparent that the mass and installation space of the sheet lamination stack have been significantly reduced. Looking at the performance values of the examined motors, it can be concluded that this scaling of the stator sheet lamination stack is not reflected in the performance values and is accordingly compensated by a more efficient design of the drive unit.

The area between the outer and the inner diameter of the stator can be divided into the slot area for accommodating the stator winding and the stator yoke. The greater reduction in the outer diameter compared to the inner diameter reduces the area available for the stator yoke and the slot area. While the slot area has changed only slightly, the yoke area has shortened. While motors from 2018 and 2019 have an average yoke thickness of 22.16 mm, this is significantly smaller for motors from 2023 at 18.55 mm. The average yoke thickness across all vehicles is 18.6 mm. The BMW iX1 xDrive30 Premium has a particularly thin yoke with 11.2 mm, while the front motor of the Tesla Model Y AWD Standard Range has the largest yoke with 27.35 mm (see Fig. 11b).

In addition to provide mechanical stability, the stator yoke is also responsible for ensuring the magnetic

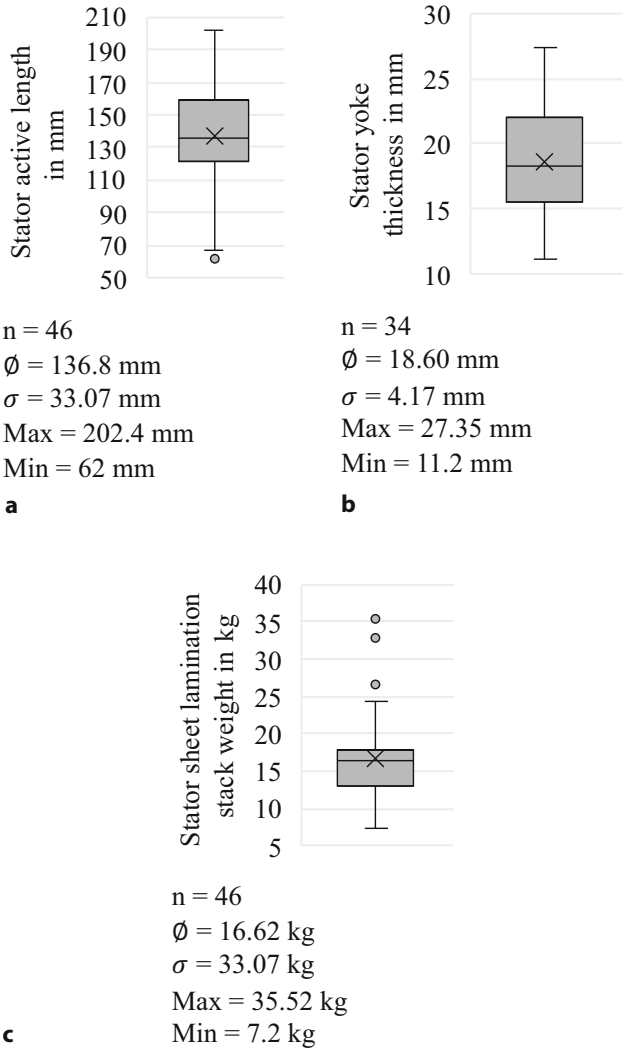



Fig. 11 Evaluation of the stator active length (**a**), of the stator yoke thickness (**b**) and of the stator sheet lamination stack weight (**c**). *n* Sample size, ∅ Average within sample, $\sigma$ Standard deviation in sample, *Max* Maximum, *Min* Minimum

flux and magnetic closure. Depending on the number of poles of the electric motor, the field lines that are conducted and amplified through the yoke are formed differently. Thus, a thicker yoke tends to be used for a lower number of poles, while a thinner yoke can be used for a higher number of poles. This relationship must be considered when selecting the yoke thickness [32].

The reduction in active length and outer diameter results in a significant weight reduction of the stator sheet lamination stack. On average, this weighed around 18.77 kg for electric motors from 2018 to 2021 and 14.81 kg for motors from 2022 and 2023. Across the entire sample, the sheet lamination stack weighs an average of 16.62 kg, with the sheet lamination stack of the MG 4 Mulan Luxury weighing 7.2 kg and that of the rear motor of the Audi e-tron 55 Quattro Edition One weighing 35.52 kg forming the lower and upper limits (see Fig. 11c).

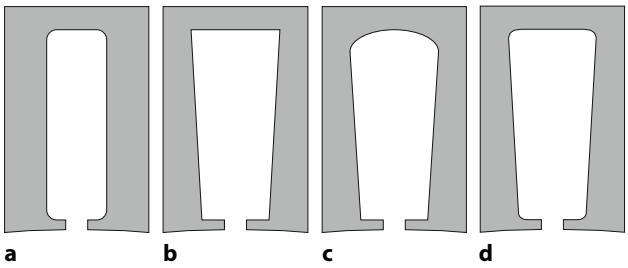



Fig. 12 Schematic representation of the slot geometries depending on the winding technology: Flat wire winding (**a**) and round wire winding (**b**) to (**d**)

**Stator winding** The main function of the stator winding is to generate a rotating magnetic field when an alternating current flows through the winding [33]. Numerous parameters can be varied to fulfil this function. Significant differences in the design of the stator winding can therefore be seen among the 48 motors examined.

Generally, the 48 examined motors have a distributed winding in which the coil extends over several teeth. Concentrated windings in which only part of a single coil is wound around a tooth cannot be identified among the 48 traction drives. 24 of the 48 motors have a stator winding made of round wire. These windings, consisting of several insulated, flexible round wires, are usually manufactured using the flyer winding and a subsequent insertion process. Due to how the winding is assembled into the stator, the winding is often named 'pull-in winding' [33–35]. To prevent the round wires from damage of the sharp edges on the top and bottom of the stator sheet lamination stack during the pull-in, edge protection can be used. This is the case with the Polestar 2 Long Range Dual Motor (2020) or the rear motor of the Mercedes EQS 580 4 MATIC AMG Line, for example.

The remaining 24 motors use flat copper wire for the winding instead of round copper wire. In this so-called flat wire winding technology, rigid, rectangular insulated flat wires are formed in a defined forming processes and afterwards axially inserted into the stator sheet lamination stack [34, 36]. Compared to round wire, flat wire offers the advantages of high power density, high copper fill factor, high efficiency at low speeds and high thermal conductivity [37, 38]. Furthermore the flat wire technology offers reduced production costs, particularly for higher quantities, due to the higher potential degree of automation [39, 40].

In addition to the numerous differences between round wire winding technology and flat wire technology, which will be discussed in more detail below, first the difference in the design of the slot shape for flat wire and round wire windings will be discussed. In all flat wire stators examined, the winding was accommodated in rectangular slots (see Fig. 12a), resulting in correspondingly trapezoidal stator teeth. For round wires, three different slot shapes could be identified within the sample, which are shown in (see Fig. 12b to d). In all three cases, the slots are trapezoidal, resulting in parallel stator teeth. The design approaches differ in terms of the shape of the wide outer edge of the trapezoid. For example, in both Audi e-tron 55 Quattro Edition One motors, there is a sharp, angular design between the slot base and the tooth flanks (see Fig. 12b). In the two BYD Tang EV motors, the wide outer edge of the trapezoid is semi-circular instead of straight (see Fig. 12c). In the rear motor of the Mercedes EQS 580 4MATIC AMG Line, a straight slot base is used similar to the Audi e-tron 55 Quattro Edition One, but the transitions to the tooth flanks are rounded (see Fig. 12d). The last two configurations with round slot ground and rounded radii with straight slot ground are the most common types of round wire motors.

Four of the motors with flat wire winding technology indicate so-called I-pin windings. Using this technology, straight copper pins, stripped at both ends, are inserted into the stator, twisted on both sides of the stator and are afterwards connected in a welding process [34, 41]. Vehicles with this type of winding are the Aiways U5 Premium, the Peugeot 208 e GT, the MG 4 Mulan Luxury and the rear motor of the Nio ET 5 Long Range (see Fig. 13a).

18 of the 24 motors that use flat copper wires feature the U-hairpin technology. Hereby, U-shaped pins are inserted axially into the stator sheet lamination stack and are twisted and welded on one side afterwards (see Fig. 13b). The elimination of welding and twisting on the other side, the so-called bending side, results in a reduction of the winding head compared to I-pin winding (see Fig. 13a, b). However, in both cases a 8 mm to 10 mm long, stripped, straight conductor is required for twisting and welding [41–44].

Both I-pin and U-hairpin are established winding technologies for traction drives in electric cars [41–43, 45]. In contrast, the X-pin technology used in the Toyota bZ4X represents an innovative further development of the U-hairpin. The bending side, i.e. the side where the bent end of the U-shaped pins is located, is identical for the X-pin and the U-hairpin. There is a difference in the structure of the welding side. Compared to the U-pin, the X-pin is manufactured with a shortened straight section at the wire end for twisting and interconnecting, resulting in reduced installation space and material usage (see Fig. 13c). However, the modified pin geometry requires process related adjustments, particularly for the twisting and contacting steps, and is significantly more complex [46, 47].

Another innovative winding topology is the so-called N-pin or Trim-cut-pin. This technology is similar to the process chain of U-hairpins, whereby after twisting the wire ends and before welding, a large part of the straight length, which is used for the twisting is cut off (see Fig. 13d). Regarding the winding head height, the Trim-cut-pin achieves similar values to the

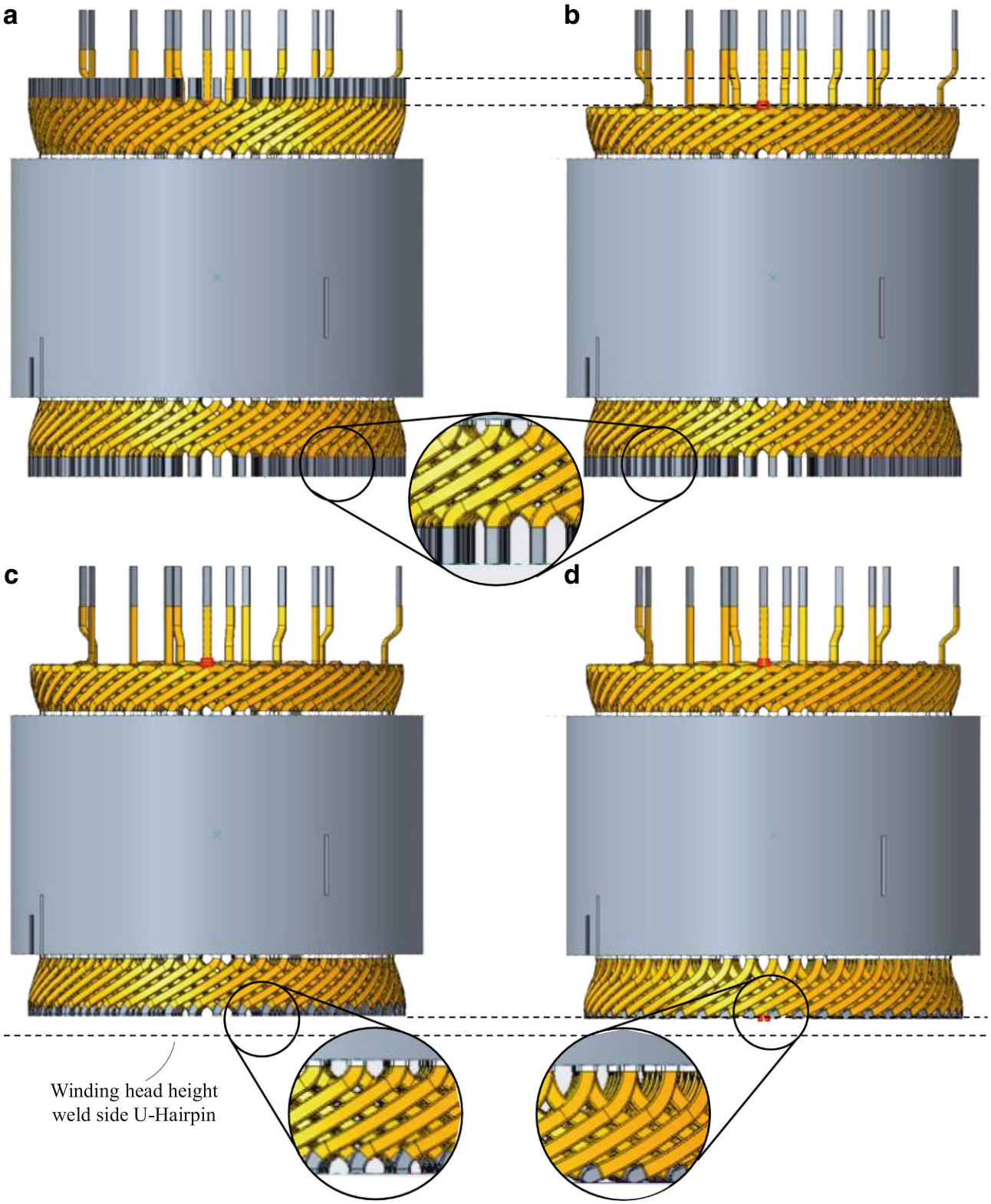



Fig. 13 Schematic representation of an I-pin stator (**a**), an U-hairpin stator (**b**), a Trim-cut-hairpin stator (**c**) and a X-pin stator (**d**) and detailed view of the welded side [47] (The representation of the I-pin was created by PEM based on a modification of the U-hairpin representation)

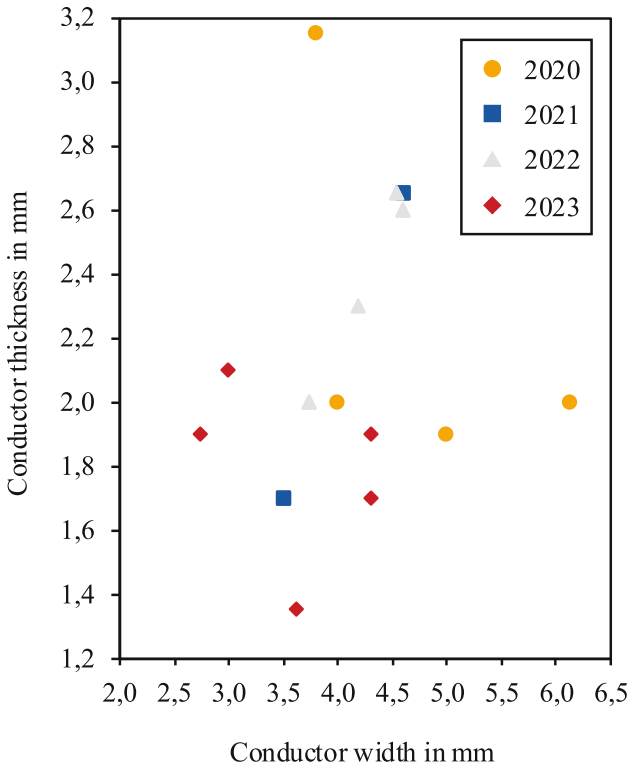



Fig. 14 Representation of the conductor width over the conductor thickness for flat wire of the stator winding depending on the model release date

X-pin, whereby the process technology is significantly less complex compared to the X-pin. The advantage of the X-pin over the trim-cut pin is the significantly higher cost savings in terms of the initial used quantity of copper. On the other hand, the complexity of industrialization and series production of the N-pin is reduced compared to the X-pin [47].

Since the winding and its properties and parameters depend on the respective technology, the analysis for round wire winding technology and flat wire winding technology is done separately. For the sake of simplicity, I-pin, U-hairpin and X-pin are grouped together here.

The stators with flat wire technology have rectangular 36, 48, 54 or 72 slots. Fifteen of the examined stators have 48 slots, followed by five stators with 54 slots. For example, stators with 36 slots are given with the front and rear motors of the BMW iX1 xDrive30 Premium, while 72 rectangular slots can be found in the Honda Advanced E and the rear motor of the BYD Seal Excellence.

In terms of the number of flat wire conductors per slot, nine vehicles have four conductors per slot, followed by eight vehicles with eight conductors per slot and four vehicles with six conductors per slot. Mostly, there is an even number of conductors in each slot. An odd number of conductors can be found in the I-pin winding of the MG 4 Mulan with five pins per slot. On average, the examined motors with flat wire have 5.88 conductors per slot.

The trend towards increasing conductor segmentation, i.e. increasing the number of conductors per slot while reducing the cross-section to reduce the negative influence of eddy currents in higher speed ranges [44, 48, 49], is clearly evident based on the sample. For example, electric vehicles from 2018 and 2020, such as the Jaguar I-Pace, Fiat 500 e La Prima and Peugeot 208 eGT, have four or two conductors per slot. The more recent models such as the Nio ET5, Smart #1, Volvo EX30 Twin Motor and Polestar 2 Long Range Dual Motor (2023), as well as the Tesla Model Y RWD, have eight or ten conductors per slot. According to this observation, all motors from 2023 have an average of 8 conductors per slot, while vehicles from 2018 to 2022 have an average of 5.17 conductors per slot.

The higher number of conductors per slot is accompanied by increasing segmentation of the individual conductors, resulting in a reduced cross-sectional area. For example, the Tesla Model Y RWD motor mentioned above, with a cross-sectional area of 4.8 $mm^2$ per conductor including the conductor insulation, has a significantly smaller area per conductor than the conductors of the Fiat 500 e La Prima winding with 12 $mm^2$. This trend is also reflected in Fig. 14, which shows the width and thickness of the conductors depending on the model year. Here, the trend towards thinner but also narrower conductors with increasing development time can be clearly observed.

The trend toward narrower and thinner conductors with smaller cross-sectional areas is due to the continuous increase in maximum motor speeds and the shift of the main operating range to higher speeds. While the first electric motors of electric vehicles such as the Jaguar I-Pace had a maximum speed of around 13,000 $min^{-1}$, newer electric motors often have maximum speeds of 20,000 $min^{-1}$ or higher. Higher motor speeds make it possible to build smaller motors with lower power consumption and less material, or to increase the overall performance of the system with the same amount of material and installation space. In both cases, the motor speed serves as a lever to increase the power density of the motor [11]. With higher motor speeds and the associated operating frequency, frequency-dependent eddy currents in the form of skin and proximity effects become more dominant in addition to frequency-independent direct current losses. To limit the former, single conductors with a reduced cross-sectional area are used.

The conductors placed in stator slots have an average cross-sectional area of 10.45 $mm^2$, including the conductor insulation (see Fig. 15a). The conductor with the largest cross-sectional area is given with the I-pin motor of the Peugeot 208 e GT with 24 $mm^2$, while the smallest conductor with 4.8 $mm^2$ is installed in the U-hairpin motor of the Tesla Model Y Standard Range RWD.

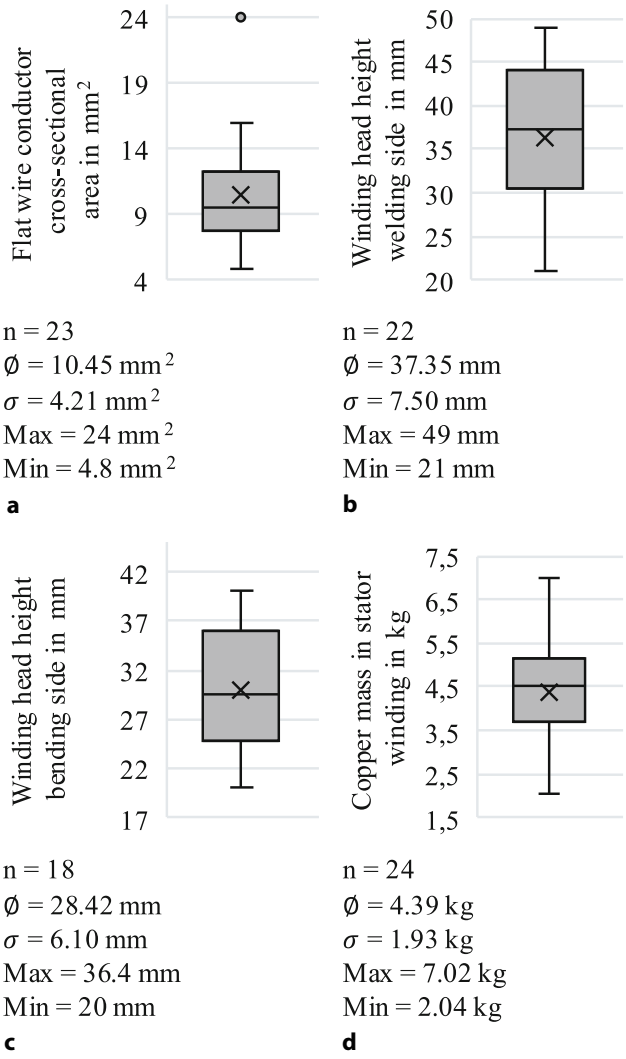



Fig. 15 Evaluation of the flat wire stators regarding flat wire conductor cross-section (**a**), the winding head heigh for the welding side (**b**), the winding head heigh for the bending side (**c**) and the copper mass in the stator winding per stator (**d**). *n* Sample size, ∅ Average within sample, $\sigma$ Standard deviation in sample, *Max* Maximum, *Min* Minimum

A wide range of materials can be identified for conductor insulation, also known as primary insulation. These include PolyEther Ether Ketones (PEEK), PolyAmide-Imides (PAI), PerFluoroAlkoxies (PFA) and PolyImides (PI). The decisive criteria for selecting the material are particularly the electrical properties in the form of partial discharge resistance or permittivity, the costs, processability/mechanical properties, thermal resistance and local and global legislation [47, 50, 51]. Regarding the trend towards 800 V+ system, PEEK is currently emerging as a primary wire insulation material [51, 52].

However, the choice of material is subject to the objective of keeping the layer thickness of the conductor insulation as low as possible while ensuring that the requirements are met over the motor lifetime. The effort to reduce the layer thickness results from the goal of maximising the amount of copper, i.e. the copper fill factor, in the slot. Within the examined flat wire conductor stators, one motor feature a PEEK insulation, 16 a PAI and seven a PI coating. The latter are primarily found in motors of Asian origin, i.e. the brands Hyundai, Toyota, MG, Smart and Volvo. Based on the sample, the trend cannot be confirmed, particularly for PEEK, which is primarily attributable to the fact that vehicles using this material as primary insulation only came onto the market after this study was completed or are still in development.

To reduce the amount of copper material used in the stator winding, efforts are made to keep the winding heads protruding at the top and bottom as small as possible. This part of the winding does not contribute to the generation of torque and serves purely to produce the desired interconnection pattern. Accordingly, a low winding head height on both sides is a decisive factor in reducing the amount of copper used and the winding resistance [33].

On the welding side, the pins for I-pins and U-hairpins are connected in the same way (see Fig. 13a, b). Accordingly, these two technologies are combined to evaluate the winding head heights for the welded side. Among the 22 flat wire motors included in the evaluation, the average winding head height for the weld side is 37.35 mm (see Fig. 15b). The minimum winding head height of 21 mm can be observed for the Honda Advanced E and the maximum height of 49 mm for the VW ID.3 1st Max. For the two X-pin stators of the Toyota bZ4X, the winding head height on the welding side is significantly lower than the average value with 23 mm.

As mentioned previously, on the bending side, the technology for X-pin and U-hairpin is identical and therefore summarised. Among the 18 motors examined, the average height on the bend side is 28.42 mm (see Fig. 15c). The minimum height is achieved by the X-pin of the Toyota bZ4X with 22.4 mm, while the maximum value of 36.4 mm is achieved by the two motors of the BMW iX xDrive50 Sport.

The height of the winding head depends largely on the shape of the hairpin. The shape of hairpins for electric motors has been frequently studied and categorised in the literature [53, 54]. Based on the classification made in Wirth et al. [53], it can be determined that F-shaped and U-shaped hairpins are primarily used in the electric motors examined. The F-shape is standard in the examined electric motors, while the U-shape is used less frequently. Regarding the exact design of the F-shape, clear differences can be seen, particularly in relation to the pronounced S-bend and the associated layer jump of the hairpin. As standard, the S-bend enables a position jump in the radial direction from one layer to a adjacent layer upstream or downstream. An extreme case of this shape can be identified in the Honda Advanced E, where the hairpin jumps over three winding layers.

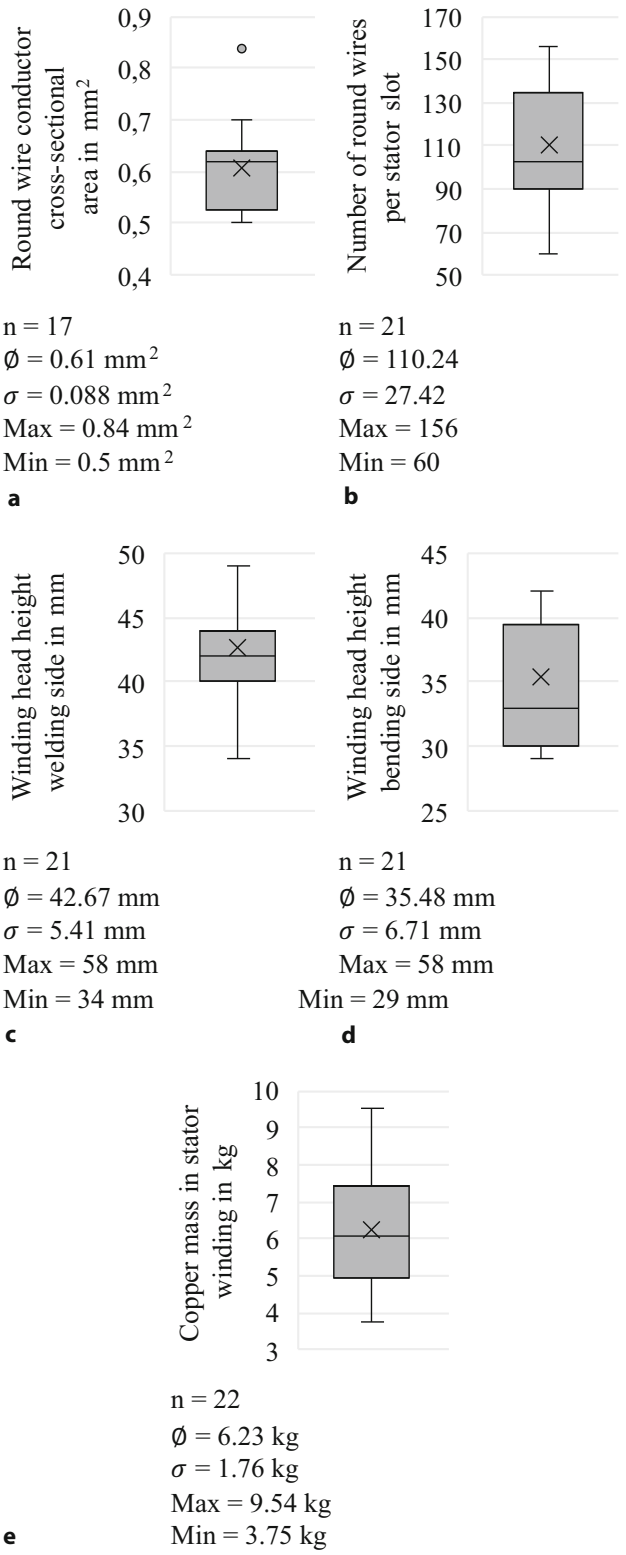



Fig. 16 Evaluation of the round wire stators regarding the round wire conductor cross-section (**a**), the number of round wires per slot (**b**), the winding head heigh for the welding side (**c**), the winding head heigh for the bending side (**d**) and the copper mass in the stator winding per stator (**e**). *n* Sample size, ∅ Average within sample, $\sigma$ Standard deviation in sample, *Max* Maximum, *Min* Minimum

The coil width in the circumferential direction, i.e. the number of slots that a hairpin skips, varies between four and nine in the sample examined. Low coil widths can be observed in motor from the years 2020 and 2021. An example is again the Honda Advanced E motor with four slots being skipped. Newer motors, such as the rear engine of the BYD Seal and the Tesla Model Y RWD engine, mostly have hairpins that skip nine slots and thus have a significantly higher coil width. Accordingly, a trend towards higher jump widths in hairpin design can be observed here.

The weight of the winding for the stator depends on numerous parameters, such as high variance in the stator diameter, conductors per slot, number of slots, conductor cross-sectional area, active length, winding head height and much more. Assuming that the insulation material accounts for 2% of the total weight of the stator windings, the average copper mass used in the flat wire examined stators is 4.39 kg (see Fig. 15d). The high dispersion of almost 2 kg can be explained by the high variance in above mentioned parameters. The largest copper mass can be observed for the stator of the VW ID.3 1st Max with 7.02 kg, while the Toyota bZ4X uses the smallest amount of copper with 2.04 kg.

As already described, 24 of the 48 stators examined are stators with a distributed round wire winding. These 24 stator windings will be examined in more detail below. In accordance with the previous description, trapezoidal slots are used instead of rectangular slots for round wire due to the smaller conductor cross-section of the individual conductors and the higher mechanical flexibility. The resulting parallel tooth flanks lead to homogeneous magnetic flux distribution in the tooth, which, in comparison to non-parallel tooth flanks in case of flat copper wires, results in lower losses or higher material utilisation of the stator sheet lamination stack [55].

The variation in the number of slots is significantly lower for round wire stators than for flat wire technology. 20 of the examined stators have 48 slots and the remaining four have 54 slots. The round wires positioned in the slots have an average cross-section, including conductor insulation, of 0.61 mm², which corresponds to a diameter of approximately 0.88 mm (see Fig. 16a).

The thickest conductor, with an area of 0.84 mm², can be detected in the front motor of the BYD Seal Excellence, and the thinnest, with an area of 0.5 mm², is given in the front and rear motors of the Audi e-tron 55 Quattro Edition One, Nissan Ariya Evolve and Renault Megane E-Tech Iconic EV 60. In terms of the development of the conductor cross-section size, no correlation with the motor topology or year of manufacture can be established.

There are an average of 110.24 conductors within a stator slot. The number of round wire conductors per slot varies within the sample between 156 conductors per slot for the rear motor of the Mercedes EQS

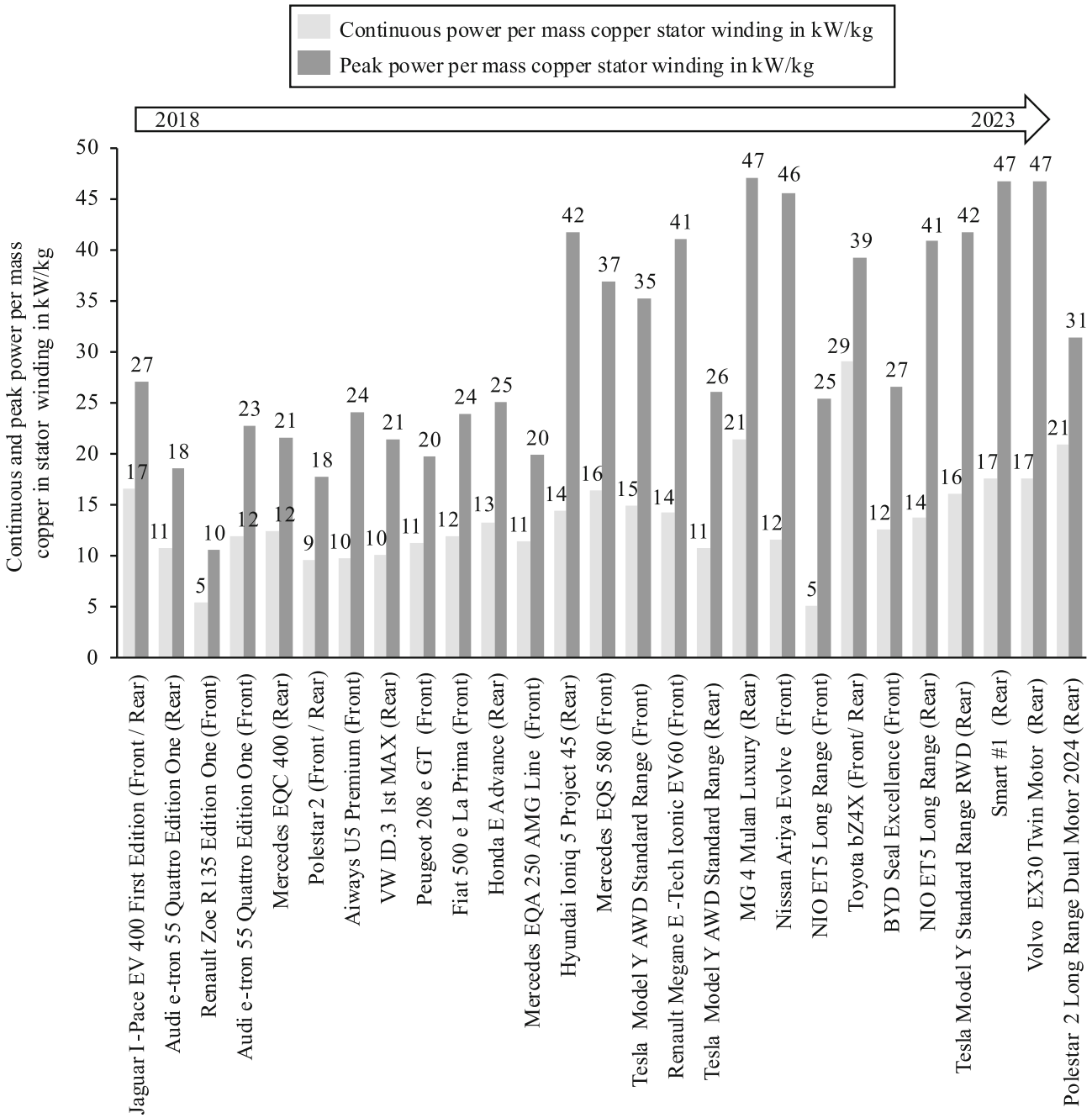



Fig. 17 Evaluation of the continuous and peak power per mass copper in stator winding

580 4MATIC AMG Line and 60 conductors per slot for the front motor of the BYD Tang EV (see Fig. 16b).

Regarding the relationship between the conductor cross-sectional area and the number of conductors per slot, a slight correlation can be observed, where the number of conductors per slot decreases as the cross-sectional area increases. However, this correlation does not apply uniformly. A counterexample is given with the front motor of the BYD Tang EV and the front motor of the Tesla Model Y AWD. The first one has 60 conductors per slot with each conductor having a cross-sectional area of 0.64 mm2, while the latter has the same conductor cross-sectional area but 120 conductors per slot. Accordingly, no clear correlation can be derived here.

In comparison to flat wire stators, round wire stators have no welding side with open wire end which need to be connected. However, to evaluate the height of the winding head, a division into the bending side and the weld side is also made here, whereby the weld side is given with the side where the end wires of the individual coils are connected.

To reduce the winding head height on the weld and the bending side and protect them against vibration, the round wires are often compressed and laced after being pulled into the stator. 22 of the 24 round

wire motors are laced, and only the two motors of the Audi e-tron 55 Quattro Edition One do not have this additional fixing element.

The winding head height for the bending side averages 35.48 mm within the sample, and 42.67 mm on the welding side (see Fig. 16c, d). For both winding head sides, the maximum winding head height of 58 mm is given by the Renault Zoe R135 Edition One. The lowest winding head height for the bending side is 29 mm for the front motor of the Audi e-tron 55 Quattro Edition One, while the lowest winding head height for the welding side is 34 mm in the front motor of the Volvo EX30 Twin Motor.

In general, it can be said that the winding head heights are 5–7 mm greater on both winding head sides compared to flat wire stators, which in turn highlights the advantage of flat wire in creating a compact winding. The installation space required for a flat wire stator is correspondingly significantly lower. In addition, the winding heads of the stator winding do not contribute to torque generation. The larger winding head heights, and thus a large amount of wire, are one of the reasons for the significantly higher average copper mass in round wire stators compared to flat wire stators. Compared to flat wire stators, round wire stators use on average 42% more copper with 6.05 kg (see Fig. 16e). The maximum copper quantity, considering a weight proportion of 5% for the conductor insulation, is 9.25 kg in the Renault Zoe R135 Edition One, which also has the largest winding head for the welded and bent sides. The lowest copper quantity is 3.63 kg observed in the Volvo EX30 Twin Motor.

Regarding the year of manufacture of the round wire motor, the models from 2018 to 2021 have a significantly higher amount of copper with an average copper weight of 7.82 kg than those from 2022 to 2023 with a value of 5.15 kg.

In course of cross-industry electrification, demand for copper and thus also the price of copper has risen significantly in recent years [56–59]. As a result, manufacturers are striving to use copper as a conductor as efficiently as possible. The effort to reduce copper usage and increase material efficiency can be seen in the fact that the amount of used copper has been reduced, regardless of topology and conductor. While this averaged 5.9 kg for vehicles in the 2018 to 2021 study, it will be 4.51 kg for vehicles from 2022 to 2023. To examine these efforts in greater detail and compare them with the performance data of the respective electric motors, Fig. 17 provides an overview of the continuous and peak power of round and flat wire motors per quantity of copper used to manufacture the winding.

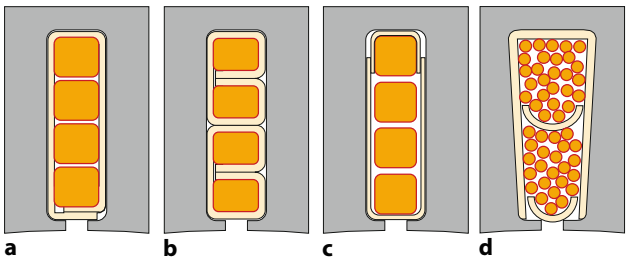



Fig. 18 Schematic representation of an identified slot insulation structures for flat wire O-shape (**a**), B-shape (**b**), U-shape (**c**) and for round wire U-shape (**d**)

The vehicles are listed according to their release year, starting with 2018 on the far left and ending with 2023 on the far right. Overall, the factor for continuous power in relation to copper weight is rising slightly. For PMSM, the factor rises continuously from 9 kW/kg for the motors of the Polestar 2 Long Range Dual Motor (2020) to around 21 kW/kg for the rear motor of the Polestar 2 Long Range Dual Motor (2023). An exception is given by the motor of the Jaguar I-Pace, which has significantly higher values than later released motors. A similar picture as for PMSM can be drawn for IMs. Starting with the Audi e-tron 55 Quattro Edition One from 2019 with 11 kW/kg and 12 kW/kg, the ratio rose to just under 16 kW/kg for the front motor of the Tesla Model Y AWD Standard Range from 2022.

An increase in the ratio can also be observed for EESM, although this value is only of limited reliability due to the small amount of available data. The Renault Zoe R135 R Edition One from 2019 has a comparatively low ratio of 5 kW/kg, but this has been significantly increased in the Renault Megane E-Tech Iconic EV60 and Nissan Ariya models from 2022 and 2023 to 14 kW/kg and 12 kW/kg.

In terms of the ratio between continuous power and copper usage, the Toyota bZ4X PMSM is particularly noteworthy. The chosen X-pin winding technology results in a low winding head height on the welding and bending side. The amount of copper that does not contribute to torque and power generation is reduced to a minimum, resulting in a particularly high ratio between continues power and used copper mass.

Regarding the ratio between peak power and the amount of copper, a significantly greater increase in the factors can be observed regardless of the motor topology. The reasons for these high increases can be manifold, for example improved cooling, optimised magnetic flux or efficient winding design. The highest ratio, with a peak power of around 47 kW/kg of copper stator winding, can be identified in PMSM, for example in the Volvo EX30 Twin Motor, Smart #1 or MG 4 Mulan Luxury. However, the EESM of the Nissan Ariya Evolve achieves a comparable value with 46 kW/kg. Compared to these two motor topologies, the factors for IMs are slightly reduced. The highest ratio for this motor topology is found in the Model Y AWD Standard Range at 36 kW/kg.

**Secondary insulation system** In addition to the insulation layer around the round or flat copper conductor, additional measures are taken to ensure the electrical functionality of the stator.

These measures include lining the stator slots with insulation paper, so called slot liner. The insulation paper serves as protection and separation of round and flat wire against the sharp-edged stator sheet lamination stack during the assembly process as well as in the later operation [60, 61]. In general, in all analyzed stators, a slot isolation paper is used. Depending on the arrangement of the insulation paper inside the slot, it also separates the individual wires within from each other. Based on the terminology used in the literature [44, 62], the O arrangement, B arrangement and U arrangement can be identified in the 48 stators for flat wires, and the U-shape can be identified for round wires (see Fig. 18a to d).

Most flat wire stators use the O-shape, which ensures that the phases of the winding are separated from the stator sheet lamination stack. The overlap of the two ends can be aligned either in the direction of the slot opening or in the yoke direction. The B-shape is only used in the older Fiat 500 e La Prima and Peugeot 208 e GT models and provides additional insulation between the conductors. However, the additional insulation protection between the pins inside the slot reduces the amount of copper that can be accommodated in the slot, which has a negative impact on the filling factor. Furthermore, the automatic production of such a fold is complex and prone to errors. The U-shape, which is only used in the two motors of the Jaguar I-pace, consists of a large and a small U-shaped profile which are pushed into each other. The assembly and material handling appear to be significantly more complex than in the O-shape. Therefore, the O-shape has become the standard for the arrangement for slot insulation.

In contrast to the flat wire stators in this study, which are mounted axially in the stator sheet lamination stack, the round wire winding is drawn into the slots from the inside of the stator, as already described. Accordingly, the slot must be opened radially before assembly and is only lined with U-shaped insulating paper at the tooth flanks as well as the slot ground. To prevent the insulation paper from shifting in axial direction during the insertion process, it is often fitted with a collar on one side. After the winding has been inserted into the slot, the slot opening is closed with a U-shaped or straight cover slide. Depending on the winding design, different phases can also be accommodated in one slot. For this purpose, a phase separator is often inserted between the two phases in the slot in round wire windings. Such a phase separator can be found for example inside the rear motor of the Polestar 2 Long Range Dual Motor (2023).

A critical parameter in the design of the insulation system is the axial protrusion of the insulation paper beyond the sheet metal package. Within the sample, the one-sided axial protrusion of the insulation paper for round wire windings is between 5 mm and 9.75 mm, with the majority of protrusions between 5.5 mm and 6.5 mm. For flat wires, the axial protrusion is slightly lower, mostly between 4 mm and 5 mm.

In addition to its use in the stator slot, insulation paper is also used in the Jaguar I-Pace, Peugeot 208 e GT and Fiat 500 e La Prima to increase the electrical strength between the stripped wire ends. To do this, a strip of insulation paper is inserted between the individual layers of the flat wire windings. Later electric motors do not feature this product characteristic.

With exception of the two motors in the Toyota bZ4X, all stators included in the study are additionally impregnated with an insulation resin. The resin impregnation fulfils multiple requirements in electric motors. By filling the air gaps in the slots of the stator, it increases the thermal conductivity from the winding to the stator sheet laminations stack, which improves the heat dissipation from the stator winding. Further, the mechanical connecting forces in the end winding and in the slot increase the overall rigidity, which has a positive effect on the NVH properties due to electric motor forces and on the motor lifetime due to lower relative movements of the stator components [63–65]. When used at axial slot ends, the electrical insulation behaviour is improved due to increased partial discharge resistance at points with local electrical field inhomogeneities [66]. Polyester, epoxy and polyetherimide-based resins are currently used as materials to fulfil these tasks. The choice of material depends primarily on the requirements for subsequent operation in terms of temperature resistance, electrical properties, desired filling level and thermal conductivity [63, 64].

Differences can be identified regarding the application location at the winding. For round wire stators, the aim is to achieve a high resin fill level both inside the slot and in the area of the winding head. This strategy is also pursued with some flat wire stators, which can be clearly seen from the discolouration of the slot liner as well as the wire insulation material caused by the resin. However, some stators are only impregnated in the stator slot, while attempting to keep the winding head as free of resin as possible. The reason for this approach could be that, due to vibration and temperature fluctuations during operation, the resin detaches from the conductor. Due to the good adhesion properties between the resin and the conductor insulation material, there is a risk that the conductor insulation will stick to the resin and be pulled off the copper core, exposing the conductor. This phenomenon subsequently leads to premature engine failure.

In the case of the Toyota bZ4X, the function of the impregnation is taken over by an expandable insulating paper. The multi-layer structure of the slot insulation paper has layers that expand when activated by heat. The insulation paper is therefore inserted into the stator like conventional paper and the winding is inserted axially. Instead of using a impregnation for mechanical fixation thermal connection between the

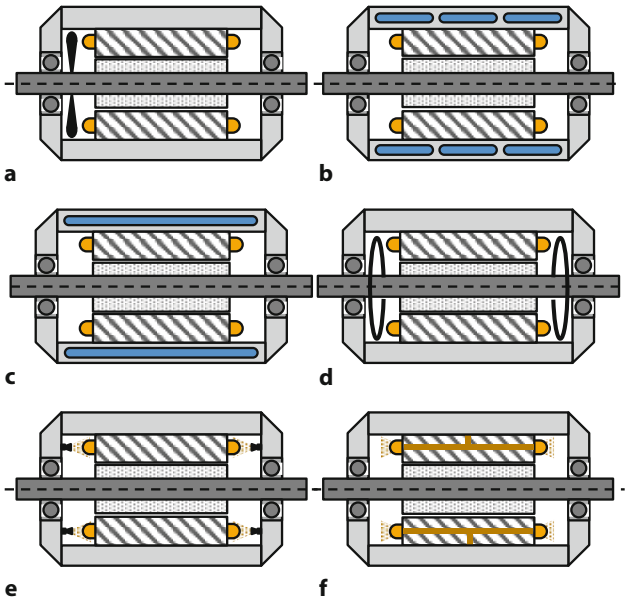



Fig. 19 Schematic representation of the cooling concepts identified within the sample: stator air cooling by fan (**a**), helical cooling jacket (**b**), axial cooling jacket (**c**), direct liquid winding head cooling with spray rings (**d**), direct liquid winding head cooling with spray nozzle (**e**) and direct liquid winding head and sheet lamination stack cooling (**f**)

stator sheet lamination stack and the winding, the material is thermally activated. This leads to an expansion of the material, filling-up the airgaps and providing a mechanical fixation and thermal connection in the same way. The impregnation process and the associated reworking and cleaning are no longer necessary [67].

Air and creepage distances play a major role, particularly in the winding head of the welded side of flat wire stators, where stripped wire ends with high potential differences are located close to each other. To ensure proper operation here, powder insulation can be identified on 11 of the 24 flat wire stators, which is usually applied using a vortex sintering process. In powder coating or vortex sintering, the wire ends are preheated and placed in a powder bath The powder touching the wire ends melts and seals the open copper sections of the wires [43]. In the case of the VW ID.3 1st Max, impregnating resin is applied to the stripped wire ends instead of a powder coating. However, the impregnation process does not generate a defined insulation layer thickness on the welded wire ends. If impregnation of the open wire ends is intended, the air and creepage distances should be designed without taking the impregnation of the open wire ends into account, and the impregnation should only be regarded as additional protection [47].

An alternative to powder coating is to encapsulate the wire ends, by which the wire ends are completely coated with a polymer and thus insulated [43]. This process can be identified in all 5th generation BMW stators and in both Toyota bZ4X stators. Especially in the case of the Toyota bZ4X stator, which has a particularly compact winding head with difficult to access stripped wire ends and very short air and creepage distances due to its X-pin configuration, the encapsulation of the stripped, welded wire ends is important for 800 V+ applications [46, 47] (see Fig. 13d).

**Stator cooling system** In general, the motor peak and continuous performance is mostly limited by thermal capabilities of several motor components. Increased motor temperature causes, for example premature failure of the insulation systems [68] or demagnetization of permanent magnets [69]. Further the electrical resistance of copper has a positive temperature coefficient, which means that as the motor temperature rises, the winding resistance increases and the efficiency of the motor decreases. Moreover a reduction in the motor installation space with the same output power results in a smaller surface area available for heat dissipation. Therefore downsizing of electric motors requires increased cooling capabilities [70–72]. These reasons highlight the importance of a functional and effective cooling system for the development of small, powerful and efficient electric motors.

Among the 48 stators examined, four different stator cooling systems can be identified, which will be discussed in the following.

A first approach, which is used in the Renault Zoe R135 R Edition One, is blowing air onto the winding and the stator sheet lamination stack by a blower positioned axially in front of the stator (see Fig. 19a). To conduct the air through the stator sheet lamination stack, holes at the outer diameter are provided. Air cooling is straightforward and enables a simple design, but due to the low thermal conductivity of air, the cooling performance is limited for applications that require higher power densities [73, 74].

A different approach involves cooling using helical (see Fig. 19b) or axial cooling channels (see Fig. 19c) in the housing or in an additional cooling jacket. Axial cooling channels are used, for example, in the Nissan Leaf Teka, the VW ID.3 1st Max, both Polestar 2 (2020) motors and both motors of the BYD Tang EV. Helical cooling channel structures can be identified in the motors of the Mercedes EQC, EQA and EQS, as well as in the motors of the Polestar 2 (2023) and Fisker Ocean 1. For simplicity, the schematic diagram is limited to cooling directly above the housing without an additional cooling jacket. In this approach the coolant flows through channels and absorbs the heat transferred from the winding via the stator sheet lamination stack. Cooling of the winding and the stator sheet lamination stack using a cooling jacket is applied in most European-manufactured vehicles. A total of 35 of the 48 stators are cooled using this cooling technology. No correlation could be identified between the use of axial or helical cooling channels in

combination with a separate cooling jacket or with channels in the housing.

Indirect cooling of the stator winding and the sheet lamination stack via a cooling jacket or cooling channels in the housing has a higher cooling capacity than air cooling but also has a limited cooling capacity due to the large distance between the heat source, given by the winding and the stator sheet lamination stack, and the heat sink, given with the channels conducting the cooling fluid. These cooling technologies prove to be disadvantageous, especially in situations where the motor is required to deliver peak power suddenly and a high amount of heat must be dissipated quickly over a long distance and numerous thermal resistances [74, 75].

To ensure sufficient heat dissipation from the stator windings and rotor parts and thus enable even more powerful motors, direct end winding cooling using electrically non-conductive coolants or gear oils has become established, particularly among Asian manufacturers. The study found nine motors with this type of cooling, including the Hyundai Ioniq 5 Project 45, Honda Advanced E, Renault Megane E-Tech Iconic EV60, Toyota bZ4X, BYD Seal Excellence and Nissan Ariya Evolve. The coolant is applied to the winding by means of spray rings (see Fig. 19d) or spray lances (see Fig. 19e)which are attached to the bearing shields. The rings and lances are thin-walled tubes with a small diameter into which the coolant is fed under pressure. The coolant is sprayed onto the winding head at specific points through fine holes in the channels. In motors using this cooling technology the stator sheet lamination stack is usually screwed into the housing for fixation and not pressed in (see Fig. 7c).

In contrast to indirect jacket cooling, direct cooling of the end wires and direct contact between the coolant and the winding as the heat source enables a significant reduction of the heat transfer resistance and transport distance. Therefore, large amounts of extracted heat result in better cooling performance. Depending on the alignment of the ring and lance, this technology can also be used to spray coolant onto the rotor, thereby cooling it as well [70, 74, 76]. As already mentioned, the application of cooling technology within the sample is limited to vehicles of Asian origin. However, numerous media reports from European manufacturers such as Audi [77] and Porsche [78] suggest that direct winding cooling will also be used in future electric motors. VW has already implemented this for the APP550, the successor to the APP310 of the VW ID.3 1st Max examined in this study [79, 80].

A further development of this technology represents the combination of direct end winding cooling with stator sheet lamination cooling. Here, the coolant is also applied to the end wires, but instead of using lances or spray rings to supply the coolant, it is fed through cooling channels in the stator lamination stack (see Fig. 19f). Accordingly, the sheet lamination stack is also cooled. Compared to direct cooling of the end windings alone, the cooling capacity can be increased, but the technical integration costs rise due to the cooling channels required, for example in the stator sheet lamination stack. This cooling technology is installed in all examined electric motors of the two Tesla Model Y models. In the case of the Tesla Model Y AWD Standard Range, the coolant is fed through a central slot in the sheet lamination stack and distributed evenly towards the two winding heads. After exiting the slot, the coolant is deflected towards the winding head via a polymer component sitting on the sheet lamination stack and applied radially from the outside to the winding. In contrast, in the Tesla Model Y RWD, the coolant is fed into the stator sheet lamination stack on one side, passed through the cooling channels through the entire stator lamination stack and then exits on the other side, where it is also directed onto the winding via the polymer ring.

**Stator interconnection** The switchgear assembly is used to transfer the 3-phase current to the stator winding. Depending on the type of connection, a distinction can be made between Y- and Δ-connections. The Y-connection is often referred to as a star connection. In theory, the Δ-connection has high efficiency at high speeds because the lower current per conductor results in lower resistance in the winding. However, the Δ-connection has low efficiency at low speeds. The Y-connection, on the other hand, shows its superiority in terms of efficiency when operated at low speeds with high torque. The lower efficiency and lower torque in the low speed range compared to the Y-connection are considered as the main disadvantages of the Δ-connection [81]. Regardless of motor topology, year of manufacture or conductor topology, all motors examined have a star/Y-connection. This

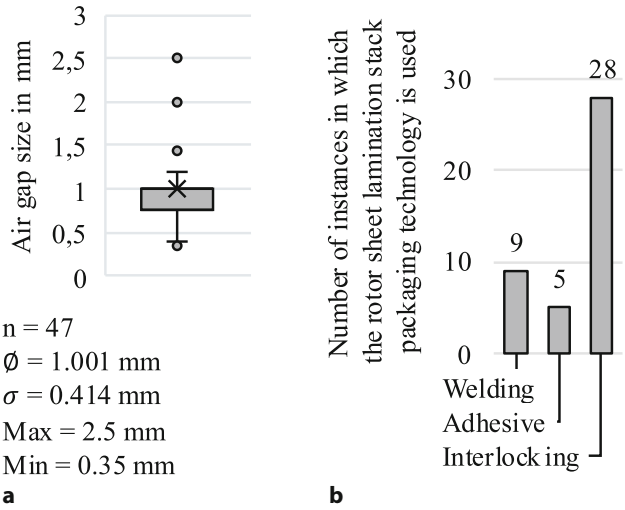



Fig. 20 Evaluation of the air gap size between rotor and stator (**a**) and used rotor sheet lamination stack manufacturing technology (**b**). *n* Sample size, ∅ Average within sample, $\sigma$ Standard deviation in sample, *Max* Maximum, *Min* Minimum

can be explained by the main speed range of today's electric vehicles, which appears to favour a star/Y arrangement in the examined vehicles.

For flat wire, the interconnection assembly usually consists of interconnection rails that run along the outer radius of the outermost winding layer or are attached to the top of the winding and connected according to the interconnection scheme. Due to accessibility in the vertical direction, extended pin ends are generally used here to ensure accessibility for the twisting, cutting to length and welding processes. The interconnection rails are often fixed in injection-moulded plastic components so that this subcomponent only needs to be placed on top or mounted on the side of the stator as a complete subassembly before the interconnection is performed. In some rare cases, the interconnection rails are individually welded to the respective pin ends and then insulated using the powder coating process. The structure and position of the interconnection assembly rails vary greatly depending on the interlocking scheme selected. In both cases, the interlocking rails are joined together so that their ends usually form three phase connections through which the stator winding the supplied with alternating current.

The interconnection assembly can be positioned on either the bending or the welding side. Within the sample, eight motors were identified in which the interconnection assembly is positioned on the bending side and 16 in which it is on the welding side. The positioning or relocation from the welding side to the bending side is achieved using special I-pins. The advantage of positioning the interconnection assembly on the bending side is given in the process control of cutting the pin ends to length and twisting before welding. In these two process steps, pins used for connection of the winding to the interconnection assembly must be treated separately due to their greater length and are usually exposed. However, if this interconnection is transferred to the bending side using additional special I-pins, this results in a uniform pin height on the welding side, which significantly facilitates the cutting and twisting processes. The disadvantage here is the additional special pin variants required for the transfer.

In round wire stators, the end wires of the individual round wire coils of the stator are brought together and connected to each other, for example by crimping. Thanks to the flexibility of the round wire, these can be laid and positioned much more freely than flat wires. The end wires usually run along the top of the winding head and are generally fixed during the lacing and compression processes of the winding head. To increase the creepage distance and insulation strength, insulation sleeves are placed over the end wires of different phases before compression and lacing.

Most motors have 3-phase connections to accommodate the aforementioned 3-phase current. Exceptions to this are the motors of the Hyundai Ioniq 5 Project 45, BYD Seal and the Renault Zoe R135 Edition One, which have a 4-phase connection. The 4-phase connection is used to utilise the inductance of the motor during charging. In case of the BYD and the Hyundai motors, by switching on the additional inductance of the motor via the 4th phase connection, it is possible to switch freely between 400 V and 800 V charging voltage according to the supply voltage of the charging station [82].

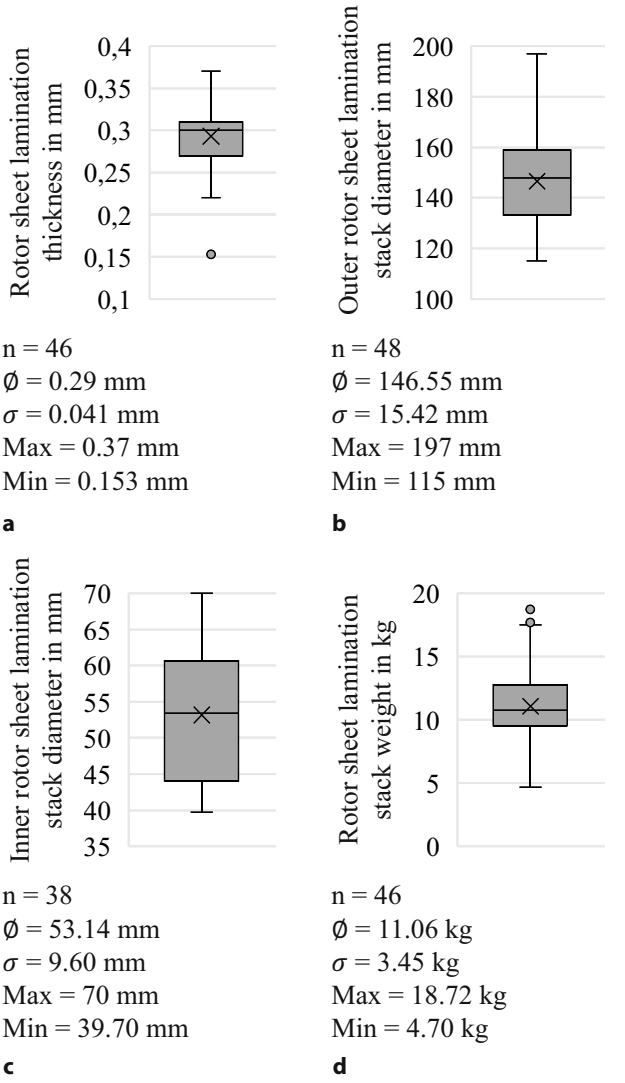



Fig. 21 Evaluation of the rotor sheet lamination thickness (**a**), the outer rotor diameter (**b**), the inner rotor diameter (**c**) and the rotor sheet lamination stack weight (**d**). *n* Sample size, ∅ Average within sample, $\sigma$ Standard deviation in sample, *Max* Maximum, *Min* Minimum

### 5.2.2 Rotor

The following subsections provide more detailed information on the structure and design of the rotor components. The first section analyzes the interface between the rotor and stator, the air gap. This is followed by a detailed analysis of the rotor components.

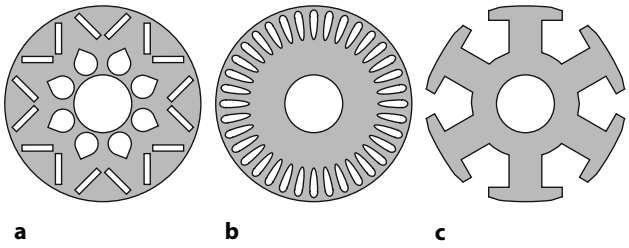



Fig. 22 Schematic representation of the rotor sheet lamination structure of a permanent magnet synchron motor (**a**), an asynchronous induction motor (**b**) and an external excited synchronous motor (**c**). *n* Sample size, ∅ Average within sample, $\sigma$ Standard deviation in sample, *Max* Maximum, *Min* Minimum

**Interface between rotor and stator** The space between the rotor and stator, which conducts the magnetic flux between the two components, is marked as an air gap. Regarding the size of the air gap, no dependence on the motor topology or the year of manufacture can be identified within the sample. On average, the air gap within the sample is 1 mm (see Fig. 20a). The maximum distance between the rotor and stator for the Nissan Leaf Teka is 2.5 mm, while the smallest air gap of 0.35 mm is found in the Honda E Advanced and Tesla Model Y RWD.

**Rotor sheet lamination stack** Like for the stator, the sheet lamination stack for the rotor is similar in terms of its external structure regardless of the motor topology and consists of a cylindrical structure made of stacked sheet laminations. Like the stator, the rotor sheet laminations are often designed as segments and then assembled into a complete rotor sheet lamination stack. The number of segments varies within the sample between 1 and 30 and shows no dependence on the year of manufacture or the height of the rotor sheet. On average, the rotor sheet lamination stacks are made up of 5 segments. The active length, i.e. the stack height of the sheets, corresponds to that of the stator sheet lamination stacks, which is why the evaluation of the active rotor is not performed individually.

As with the stator, the individual sheet laminations must be joined together, whereby welding, adhesive bonding and interlocking can be identified as packaging technologies (see Fig. 20b). The latter method is the most used, and in two-thirds of the rotors examined, the sheet laminations are joined together by interlocking. The second most used technology, accounting for around 20%, is welding the sheets together. As with stator sheet lamination stacks, this process offers high productivity and high mechanical integrity but has product-related disadvantages due to the creation of a short-circuit edge. The process is used exclusively to join the sheets for EESM rotors, with the weld seam being placed at the transition between the rotor teeth and the central rotor joke. The alternative method of bonding the sheets is used in five of the analyzed rotors. A combination of two packaging technologies, as for the stator sheet lamination stack packaging, could not be identified.

The evaluation of the sheet lamination thickness including the surrounding insulation layer shows that the average sheet lamination thickness is 0.29 mm (see Fig. 21a). Compared to the average sheet lamination thickness of 0.3 mm for the stator, this is a comparable value. The minimum and maximum values are 0.153 mm for the rear motor of the Nio ET5 and 0.37 mm for the Peugeot 208 e GT. As with the stator, there is a trend towards thinner sheets to reduce eddy current losses in the sheet stack. While the vehicles from 2018 and 2022 have an average sheet lamination thickness of 0.31 mm, this is lower for the vehicles from 2023 at 0.26 mm.

The outer diameter of the rotor stack structure is derived from the inner diameter of the stator and the air gap discussed in the previous section. On average, the sheet metal under consideration has an outer diameter of 146.55 mm (see Fig. 21b). In line with the previous descriptions of the stator diameter, IM motors have a larger stator diameter, which also results in a larger rotor diameter. Regardless of this consideration, the largest rotor outer diameter is found in the Honda E Advance at 197 mm, and the smallest diameter is 115 mm for the front motor of the Volvo EX30 Twin Motor. As with the stator diameter, dependencies on the motor topology can also be observed for the rotor outer diameter. This results in an average value of 149.44 mm for IM, while the values for PMSM and EESM are slightly lower at 145.3 mm and 147.78 mm.

The inner diameter of the rotor forms the interface to the rotor shaft and averages 53.14 mm (see Fig. 21c). No dependencies on motor topology or other characteristics can be identified for the inner diameter. The

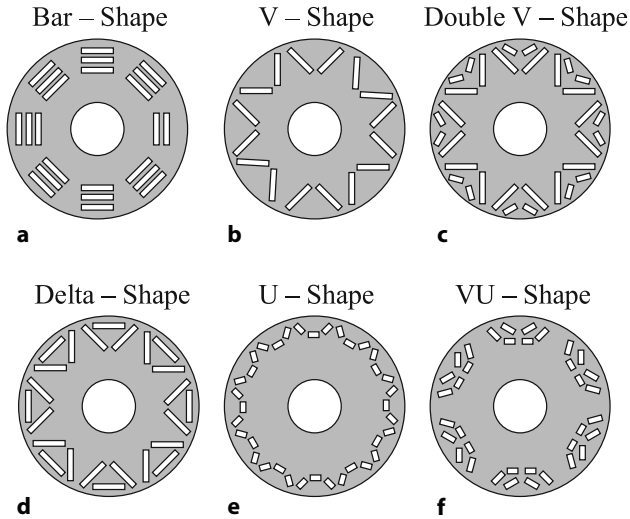



Fig. 23 Schematic illustration of permanent magnet arrangement: Bar-Shape (**a**), V-Shape (**b**), Double V-Shape (**c**), Delta-Shape (**d**), U-Shape (**e**) and VU-Shape (**f**). *n* Sample size, ∅ Average within sample, $\sigma$ Standard deviation in sample, *Max* Maximum, *Min* Minimum

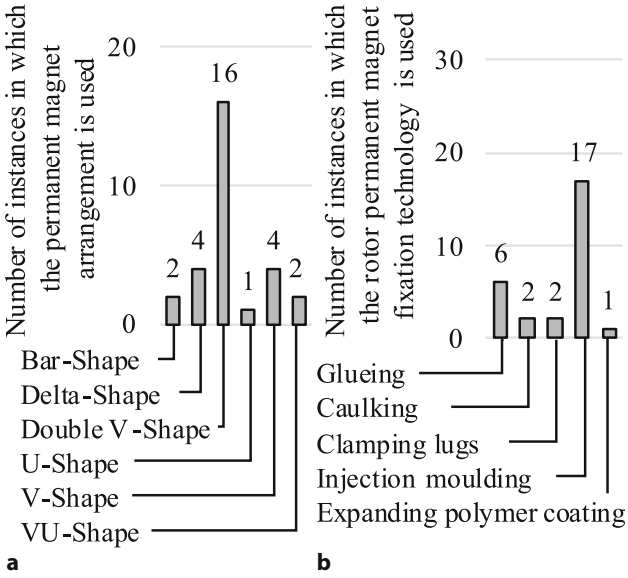



Fig. 24 Evaluation of the rotor permanent magnet arrangement (**a**) and used rotor permanent magnet fixation technology (**b**). *n* Sample size, ∅ Average within sample, $\sigma$ Standard deviation in sample, *Max* Maximum, *Min* Minimum

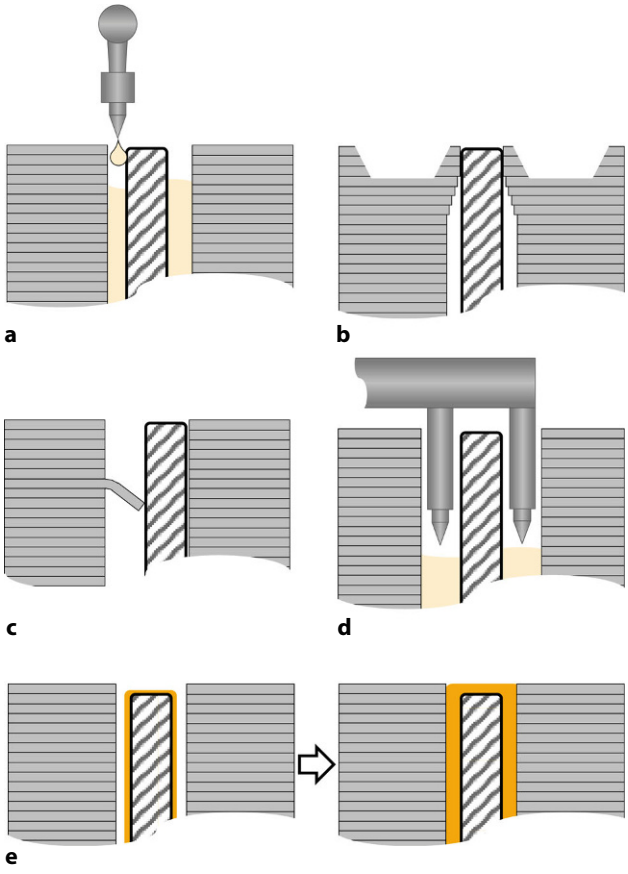



Fig. 25 Schematic illustration of identified concepts for magnet fixation inside the rotor sheet lamination stack: Glueing (**a**), Caulking (**b**), Clamping lugs (**c**), Injection molding (**d**) and expanding polymer coating (**e**). *n* Sample size, ∅ Average within sample, $\sigma$ Standard deviation in sample, *Max* Maximum, *Min* Minimum

maximum value of 70 mm is found in the front motor of the Tesla Model Y AWD, and the minimum value of 39.7 mm is found in the front motor of the Volvo EX30 Twin Motor.

While the outer structure is identical regardless of the rotor topology, the design of the individual sheets differs significantly in terms of the position, size and number of punchings. Sheet metal from PMSMs has cut-outs to accommodate the permanent magnets and to utilize the reluctance torque (see Fig. 22a). The cut-outs are evenly distributed in whole number repetitions over the entire surface. The rotor sheet lamination stack for IMs has droplet-shaped cut-outs in the outer area of the sheet lamination stacks to prevent short-circuit bars (see Fig. 22b). The sheet lamination stack for EESM rotors has an inner yoke to which numerous teeth are connected, on which the rotor winding is placed (see Fig. 22c).

Both the design of the sheet lamination and the outer structure have an influence on the total weight of the component. On average, all rotor sheet lamination stacks weigh 11.06 kg (see Fig. 21d). The maximum rotor sheet weight within the sample is 18.72 kg for the rear motor of the Mercedes EQC 400 4MATIC 1886 Edition. The minimum weight can be identified for the motor of the MG 4 Mulan at 4.69 kg.

The analysis of the data shows that the rotor sheet lamination stacks of the IM stand out regarding their high weight. This results in an average weight of 13.75 kg for IM. The high weight can be attributed to the larger outer diameter compared to EESM and PMSM. In addition, the IM rotor sheet lamination stacks only have small recesses on the outer radius, whereas the stack for PMSM or EESM have significantly larger recessed areas, resulting in a lower weight.

EESM rotor sheet lamination stacks have an average weight of 11.34 kg, with the maximum of 13.982 kg being achieved by the Renault Zoe R135 Edition One and the minimum of 9.69 kg by the rear motor of the BMW iX1 xDrive30 Premium. For PMSM, the average weight is 10.11 kg. The fact that the weight of the EESM rotor sheets is higher than that of the PMSM sheets despite the large cut-outs between the rotor teeth can be attributed, for example, to the higher active length of EESMs compared to PMSM stators.

**Rotor balancing** To compensate for possible imbalances in relation to the axis of rotation, rotors are balanced before being installed in the stator. Mostly, this is done by using a subtractive balancing process, for example a drilling device to remove a defined amount of material from the rotor's seating surface at a defined diameter and thereby compensating for the detected imbalance. This procedure has been used on 91% of the rotors inspected. In the remaining 9%, additive balancing was performed, i.e. a defined amount of

material was added at a designated point in accordance with the detected imbalance. Examples of the much less common additive balancing can be found in the front and rear motors of the Mercedes EQS 580 4MATIC AMG Line and the Polestar 2 (2020). In both cases, cylindrical defined mass elements are inserted into recesses in the sheet lamination stack. The recesses are located in the area between the short-circuit bars or the recesses for the permanent magnets and the inner rotor diameter.

In case of subtractive balancing, holes are drilled into the balancing disc mounted on the side of the rotor in 36 of the 47 rotors. An alternative to this is to remove material from the rotor sheet lamination stack using a drilling unit. This alternative has been implemented for all motors in the BMW iX, i7 and iX1 models and the front motor of the Polestar 2 (2023).

In the following, a distinction will be made between the three motor topologies found in the sample to be able to discuss the specific properties of each topology.

**Permanent magnet synchron rotor** The rotor sheet lamination stack for the PSMS has recesses in which magnets are arranged. Numerous different arrangement techniques can be identified. An overview of the possible designs,the number and frequency with which the respective structure is used is shown in Fig. 23a to f. The evaluation of the distribution of the technology within the sample is shown in Fig. 24a.

In the case of the Bar-Shape, which is found exclusively in the two Jaguar I-Pace rotors, several identical magnets are arranged in a straight line one behind the other (see Fig. 23a). In the V-Shape, two identical magnets are arranged at an angle to each other in a V-Shape (see Fig. 23b). This arrangement can be found, for example, in the PMSM of the two Tesla Model Y models. The most used topology is the Double V-Shape arrangement, in which four magnets are arranged in two rows behind each other in a V-Shape (see Fig. 23c). This topology has been used in vehicles since 2021, such as the Volvo EX30, Nio ET5 and BYD Seal Excellence.

A structure like the V-Shape is the Delta-Shape, in which the V-Shaped opening of two magnets is closed by a third magnet (see Fig. 23d). This structure can be found in four of the 29 PMSM rotors examined, such as the Nissan Leaf Tekna and the two BYD Tang EV motors. In the U-Shape, which is only found in the Honda E Advanced, several magnets are arranged in a U-Shape (see Fig. 23e). This topology can be combined with the V-Shape, as in the two Toyota bZ4X motors, for example, with form the VU-Shape (see Fig. 23f).

The different arrangement topologies require between one and four magnet types with different dimensions. For the Bar-Shape, V-Shape and U-Shape topologies, only one magnet type is generally used. For the Delta-Shape and Double-V-Shape, two different magnets are generally used. An exception to this is the rear motor of the BYD Seal Excellence, which uses a total of four magnet types. In this special case, the magnets used in two adjacent segments differ.

The total number of magnets per rotor varies between 48 and 360, with an average of 141. The number of 192 magnets is often combined with the double V-Shape, while 48 are often combined with the V-Shape or VU-Shape, as in the Tesla Model Y. The maximum number of 360 magnets can be found in the Honda E Advanced.

Five different methods are used to fix the position of the magnets within the rotor sheet lamination stack for the analyzed rotors (see Fig. 24b and Fig. 25). For gluing, which is used in the two Jaguar I-Pace motors, adhesive is applied to the cavity in the rotor sheet lamination stack or to the magnets themselves before assembly, which is then cured under heat to fix the magnets in place (see Fig. 25a). An alternative to this is caulking the magnets, implemented in both BYD Tang EV rotors. Here, the magnets are pre-mounted in the sheet. A tool is then used to mechanically deform the sheets near the magnets (see Fig. 25b). The mechanical deformation of the sheet stack fixes the magnets in the slots. Several small deformations or one large deformation can be used to deform the rotor sheet. The deformation can be circular or square in shape. A mechanical alternative is the application of a clamping lug. This process is used in both Tesla Model Y PMSMs. Here, certain sheet laminations of the rotor sheet lamination stack are provided with a spring at regular intervals, which extends into the mounting slot of the magnet. When the magnet is inserted into the recess, the clamping lugs are deformed and fix the magnet in place via the spring force (see Fig. 25c).

The most used alternative is injection moulding, in which the magnet is completely encased in a polymer in the slot. To ensure sufficient encapsulation, recesses are usually provided for the injection moulding tooling (see Fig. 25d). To increase the volume of the permanent magnets mass and improve the magnetic flux, bonded permanent magnets can be used instead of a polymer in the injection moulding process. This combination of sintered permanent magnets in the recess and bonded moulded magnets for fixing in the free spaces around them is also referred to as a hybrid rotor assembly [83].

A final fixation alternative is the use of an expanding coating. Here, the magnet is coated with a thermally expandable compound before being installed in the sheet lamination stack. After installation and pre-fixing in the sheet lamination stack, the expansion process is initiated in a heating process. The expansion of the coating fixes the magnet within the slot. This process is used in the rotor of the VW ID.3 1st Max (see Fig. 25e).

The magnets can be additionally fixed by subsequently roll-dipping the fully assembled rotor in

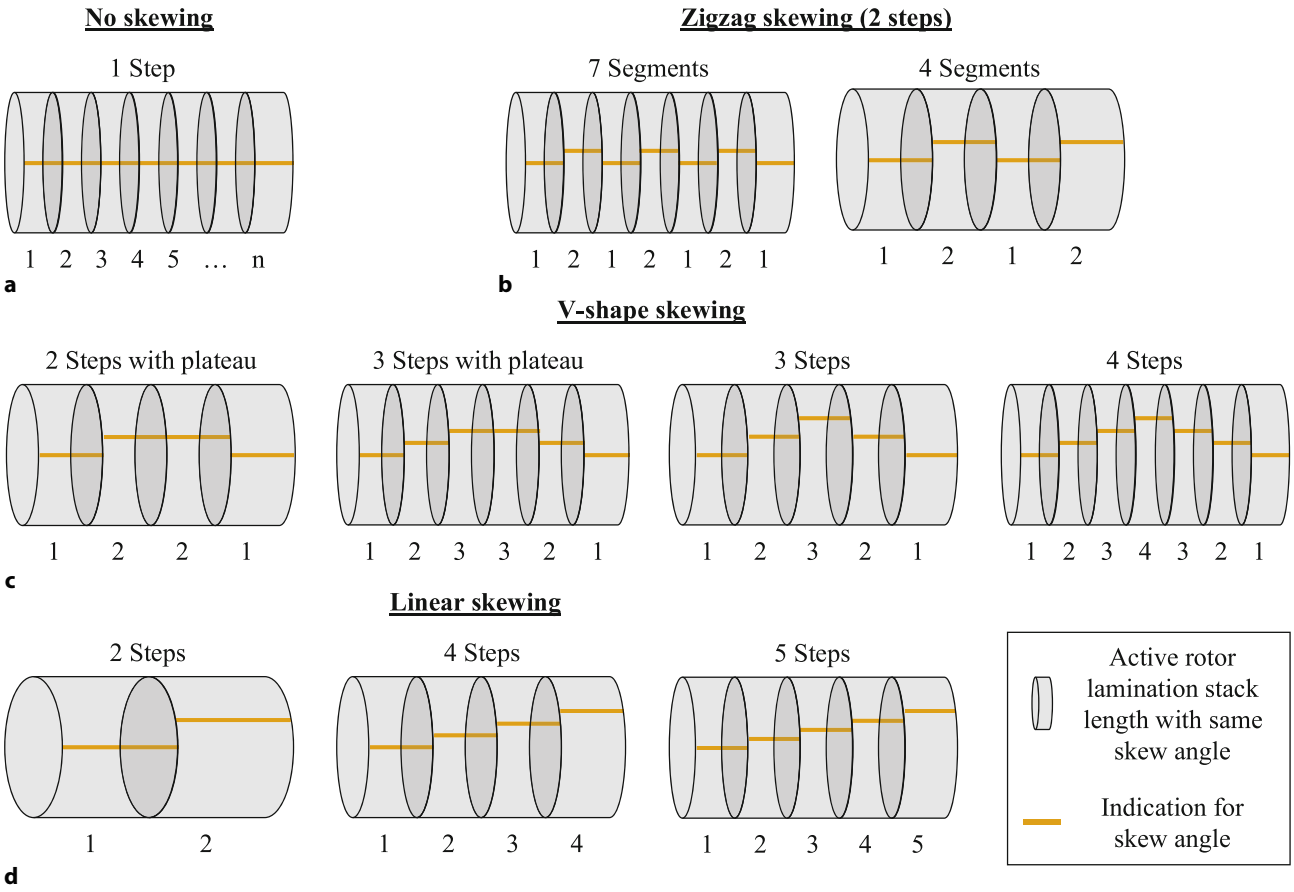



Fig. 26 Schematic representation of the different skewing techniques identified in the analyzed sample: No skewing (**a**), Zigzag skewing (**b**), V-shape skewing (**c**) and linear skewing (**d**). *n* Sample size, ∅ Average within sample, $\sigma$ Standard deviation in sample, *Max* Maximum, *Min* Minimum

a resin bath. During roll dipping, the rotor is impregnated with resin material, which stiffens the entire structure in a subsequent curing process. The fully impregnation of a PMSM rotor can be identified for the front motor of the Volvo EX30 Twin Motor but is not otherwise widely used.

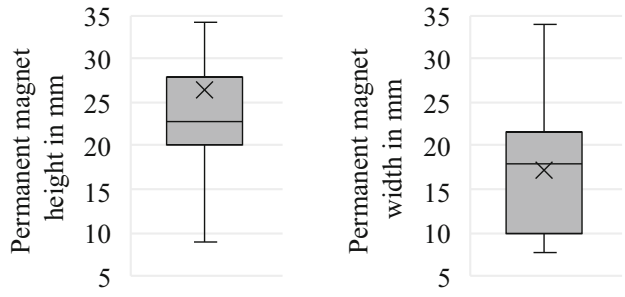
The PMSM rotor of the BYD Excellence was the only rotor in which no additional mechanism for fixing the magnets could be identified. Accordingly, it can be assumed that no additional measures were taken to fix the magnets in their positions in this rotor sheet lamination stack.

As already mentioned, the magnets are usually fixed in the rotor sheet lamination stack segments using the technologies described above and then stacked on top of each to the intended active length. During stacking, the rotor sheet lamination stack segments are often rotated at a certain angle to each other, which is called skewing. Skewing serves to reduce and optimize torque ripple and radial electromagnetic vibrations. Possible design variables here are the absolute angular offset between adjacent rotor sheet lamination stack segments, the general topology of the angular offset and the number of segments [84–86]. Based on the investigation of the PMSM rotors in the sample, four higher-level techniques with numerous different details can be identified in accordance with the terminology used in the literature, which will be discussed in more detail below (see Fig. 26).

Seven of the 29 motors examined, including the motors of the Honda E Advanced, the Polestar 2 (2020), the Mercedes EQS 580 and the Toyota bZ4X, do not exhibit any skewing (see Fig. 26a). Accordingly, there is only one level on which all magnets are arranged or to which all magnets are aligned. The number of segments varies between 4 for the front motor of the Mercedes EQS 580 and 10 for the Honda E Advanced.

In the case of Zigzag skewing, rotor segments are alternately aligned on two offset planes with a constant angular offset relative to each other (see Fig. 26b). Within the study, three vehicles can be identified with this technology, with the motors of the Hyundai Ioniq 5 Project 45 featuring four segments and the motor of the Peugeot 208 e GT featuring seven stages.

Most of the vehicles in the study are designed according to the V-shape skewing (see Fig. 26c). Here, the rotor sheet lamination stack segments are rotated relative to each other in such a way that the overall view forms a V. Differences exist in the number of



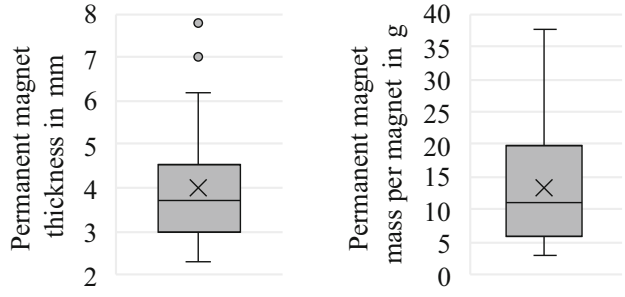

n = 47
∅ = 26.5 mm
$\sigma$ = 13.48 mm
Max = 78 mm
Min = 8.9 mm

**a**




n = 47
∅ = 17.14 mm
$\sigma$ = 6.4 mm
Max = 34 mm
Min = 7.7 mm

**b**



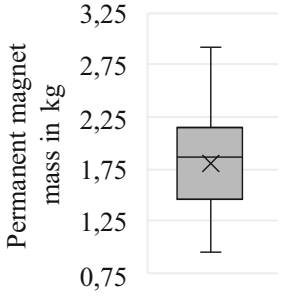

n = 47
∅ = 4.00 mm
$\sigma$ = 1.2 mm
Max = 7.8 mm
Min = 2.3 mm

**c**




n = 47
∅ = 13.26 g
$\sigma$ = 8.31 g
Max = 37.5 g
Min = 2.8 g

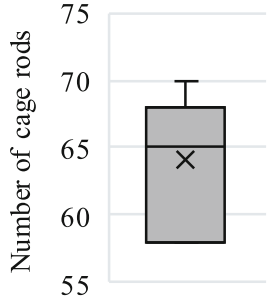
**d**




n = 28
∅ = 1.81 kg
$\sigma$ = 0.49 kg
Max = 2.91 kg
Min = 0.96 kg

**e**

Fig. 27 Evaluation of the characteristics aspects of the used permanent magnets regarding the height (**a**), the width (**b**), the thickness (**c**), the magnet mass per magnet (**d**) and the permanent magnet mass per rotor (**e**). *n* Sample size, ∅ Average within sample, $\sigma$ Standard deviation in sample, *Max* Maximum, *Min* Minimum




n = 8
∅ = 64.11
$\sigma$ = 4.63
Max = 70
Min = 58

**a**




n = 9
∅ = 2.26 kg
$\sigma$ = 0.64 kg
Max = 3.83 kg
Min = 1.57 kg

**b**

Fig. 28 Evaluation of the number of cage rods (**a**) and the rotor cage mass (**b**). *n* Sample size, ∅ Average within sample, $\sigma$ Standard deviation in sample, *Max* Maximum, *Min* Minimum

steps into which the V is segmented and in whether there is a plateau in the middle consisting of two segments with the same rotation. The two- and three-stage variants with plateau are the most used topologies. V-shape skewing is used, for example, in all Tesla, BYD, Volvo, Jaguar Nio, Smart and Fisker PMSMs.

The second most used technique is linear skewing (see Fig. 26d). Here, adjacent segments are constantly twisted at a certain angle to each other so that, when viewed as a whole, there is a linear increase from one rotor end to the other. Overall, this technique is used in five PMSMs, including the VW ID.3 1st max, the MG 4 Mulan Luxury and the Polestar 2 (2024).

Regarding a trend towards a specific skewing topology, it can be observed that the majority of vehicles from 2022 and 2023, and almost all vehicles from

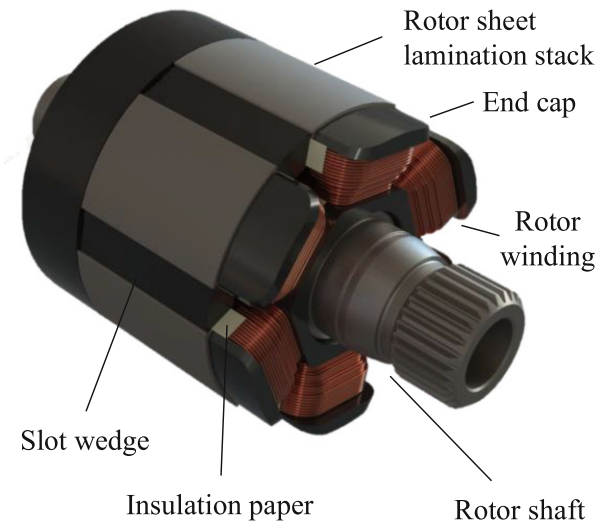



Fig. 29 Schematic representation of an external excited synchronous machine

2023, exhibit V-shape skewing topology. Accordingly, a trend towards this topology appears to be emerging.

Almost all magnets used in rotors are rectangular and, in rare cases, square. Mostly the height of the magnets corresponds to the height of the rotor sheet lamination stack segment. This means that after stacking the sheet lamination stack segments, the magnets can be mounted and then several segments can be assembled into a complete rotor. On average, magnets have a height of 26.5 mm in the axial direction of the rotor, a width of 17.14 mm and a thickness of 4 mm. However, due to the different arrangements of the magnets and the variations in the number and height of the sheet lamination stack segments, these parameters vary greatly. For example, the Honda E Advanced has particularly small magnets with dimensions of 9.1 mm x 7.9 mm × 6.2 mm [height × width × thickness], while the PMSM of the Tesla Model Y AWD has dimensions of 33 mm × 22 mm × 7 mm [height × width × thickness] (see Fig. 27a to c).

Due to the variation in dimensions depending on the topology, there is also a variation in weight per magnet. On average, the magnets used weigh 13.26 g, with the largest and smallest weights of 37.5 g and 2.8 g found in the Tesla Model Y AWD and Honda E Advanced mentioned above (see Fig. 27d).

Based on the geometry of the magnets and their arrangement in cross-section, this results in a total permanent magnet mass of 1.81 kg per rotor. The maximum magnet mass is 2.91 kg for the rear motor of the Mercedes EQS 580 and 0.96 kg for the front and rear motors of the Toyota bZ4X (see Fig. 27e).

**Asynchronous induction rotor** In the case of the Audi e-tron 55 Quattro Edition One, IM can be used as the main drive in combination with another IM or, as in the BYD Seal Excellence example, as an auxiliary drive (see Appendix Table 1). Like the PMSM, the motor consists of a sheet lamination stack, but instead of permanent magnets, a short-circuit cage is mounted. The short-circuit cage is usually made of aluminum or copper, although all eight motors examined in the sample were made of aluminum. The short-circuit cage consists of two short-circuit rings positioned above and below the sheet lamination stack and numerous short-circuit bars embedded in the recesses in the sheet lamination stack. Such aluminum short-circuit cages are usually manufactured using a casting process. The short-circuit rings on the top and bottom of the sheet lamination stack are often provided with a blade structure on the end face, which ensures additional air circulation during operation and thus a cooling effect. The short-circuit rings in the sample had a height of between 14 mm and 25 mm (see Fig. 28a). The number of short-circuit bars per rotor varies within the sample between 70 and 58, with an average of 64.11. The maximum number of 70 is found in the Tesla Model Y AWD Standard Range, and the lowest number of 58 is found in the two Audi e-tron 55 Quattro Edition One motors and the Nio ET5 Long Range. To reduce torque ripple and improve NVH behavior, the copper rods can be angled in a similar way to the permanent magnets. In this case, the axis of the short-circuit rods does not run parallel to the motor axis but at an oblique angle.

Within the sample, the average aluminum mass used for the short-circuit cage is 2.26 kg, with the maximum amount of 3.83 kg found in the rear motor of the Audi e-tron 55 Quattro Edition One and the minimum amount of 1.57 kg in the Tesla Model Y AWD Standard Range (see Fig. 28b).

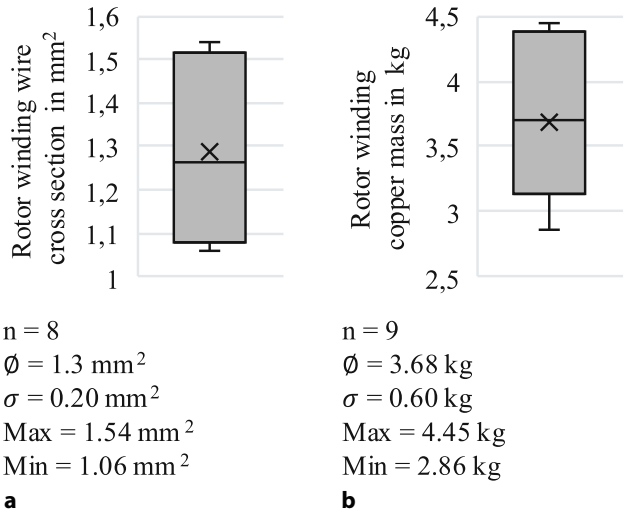



Fig. 30 Evaluation of the rotor winding wire cross section (**a**) and the rotor winding copper mass (**b**). *n* Sample size, ∅ Average within sample, $\sigma$ Standard deviation in sample, *Max* Maximum, *Min* Minimum

**Externally excited synchronous rotor** The last rotor topology identified in the sample is the EESM. To visualize and explain the structure of the motor topology, a generic externally excited synchronous machine is shown in Fig. 29.

The sheet lamination stack is designed with a central yoke and rotor teeth and slots evenly distributed around the outer radius. Concentrated round wire coils are wound around these teeth in all rotors examined. The Renault Zoe R135 Edition One is equipped with four rotor teeth, all BMW EESMs have six teeth, and the motors of the Megane E-Tech Iconic EV60 and Nissan Ariya Evolve have eight teeth. In the active length of the rotor sheet lamination stack, the winding is separated from the stack using an insulating paper, which is 0.6 mm thick in the BMW rotors. To protect the winding and its insulation from the sharp edges on the top and bottom of the sheet lamination stack, end caps are placed on the top and bottom before winding. These have a similar basic contour to the rotor sheet lamination stack but have rounded edges in the area of the slots and rotor teeth so that the wire runs tangentially into the slot and does not come into contact

with the upper and lower edges of the sheet lamination stack. This is usually an overmoulded aluminum profile, as found on the BMW iX xDrive50 Sport or Renault Zoe R135 Edition One. The end caps are usually fixed to the sheet lamination stack via recesses in the sheet laminations.

In all nine rotors examined, power is transferred from the battery to the rotor winding conductively via sliding brushes and copper sleeves. To further secure the position of the insulation paper and the rotor winding, cover slides are inserted between the rotor teeth. In addition, all EESM rotors from BMW are completely encapsulated with a casting resin for fixation and to increase the thermal conductivity between the components. In this case, the cover slides fulfil the additional task of sealing the rotor and preventing the casting compound from running out before it hardens. Unlike the BMW rotors, the rotors of the Megane E-Tech Iconic EV60, the Nissan Ariya Evolve and the Renault Zoe R135 Edition One are not completely encapsulated but only impregnated with an impregnating resin to ensure mechanical integrity.

The winding has been applied directly to the rotor teeth in all rotors using needle, flyer or linear winding. The wire used, including insulation, had an average cross-sectional area of 1.3 $mm^2$ (see Fig. 30a). The maximum cross-sectional area is 1.54 $mm^2$ in the BMW i7 xDrive60 Individual, while the minimum cross-sectional area is 1.06 $mm^2$ in the Nissan Ariya Evolve and Megane E-Tech Iconic EV60. Assuming that the insulation material accounts for 5% of the total weight, the average total copper mass for the rotors is 3.68 kg. The largest copper mass is found in the BMW i7 xDrive60 Individual at 4.45 kg, and the smallest in the BMW iX1 xDrive30 Premium at 2.86 kg. (see Fig. 30b).

**Reduction gear** Based on the analysis of the topology and arrangement of motor housing, transmission and power electronics, the transmission is flanged to the side of motor housing. Seven of the vehicles examined use a planetary gearbox to reduce the high speed of the motor to the lower wheel speed at high torque. Examples of drive units with a planetary gearbox are the engines of the Jaguar I-Pace and the two Polestar 2 models. The remaining 41 motors feature a conventional spur gear. Regarding the transmission topology used and the overall structure of the drive unit, all motors with a planetary gear can be assigned to the two topologies shown in Fig. 2c, d.

## 6 Summary and conclusion

This article provides a comprehensive overview of the development of traction motors based on an analysis of 48 traction drives from a total of 31 electric vehicles from 2018 to 2023. For this purpose, the topology of the drive units was first analyzed and classified in terms of power-to-weight ratio. This was followed by a detailed product and production technology analysis at the component level. In course of this, a classification was made regarding the current component structure and, in addition, design and manufacturing trends were derived, discussed and analyzed. The data provided and undertaken analysis serve as an overview of the state of the art and current trends for the next generation of traction motors in electric vehicles.

Some of the key findings and trends can be summarized as follows:

The drive unit, consisting of motor, gearbox and power electronics, is increasingly being designed as a compact and integrated structure. Housing components from the motor, gearbox and power electronics are integrated into one another to reduce interfaces, assembly work, the number of basic components required and the overall weight, and to increase the efficiency of material use. This usually comes at the expense of the complexity of the manufacturing processes for these structures.

The effort to reduce material usage and thereby increase material efficiency can also be observed for the rotor and stator sheet lamination stack. Lighter and smaller sheet lamination stacks are used here to reduce weight and material usage. To increase the efficiency of the used material, the trend here is towards ever finer sheet laminations to reduce losses during operation. This trend can also be observed in the field of stator winding. New winding technologies such as the X-pin are being used to reduce the winding head height on both sides and initially reduce the amount of copper used.

As described, the peak and continuous power of the engine is limited by the thermal properties of various engine components. In order to enable increased peak and continuous power with the same materials, oil cooling systems are increasingly being used, particularly in Asia, as they offer increased cooling performance compared to conventional jacket cooling systems.

Function integration as a means of reducing material usage can be identified not only in the general housing structure but also at the component level. For example, the Toyota bZ4X uses an expanding insulation paper that combines the functions of slot base insulation and secondary impregnation in a single component, eliminating the need for secondary impregnation of the stator. This reduces both manufacturing costs and investment in plant technology. Another example is the clamping of the permanent magnets in the rotor using clamping lugs integrated in the design of the sheet laminations. This eliminates the need for an additional process to secure the magnets, e.g. by glueing or injection moulding.

**Funding** This work is part of the research project Scale-up E-Drive (funding indicator: 16THB0006E) funded by the

German Federal Ministry for Economic Affairs and Climate Action.

**Funding** Open Access funding enabled and organized by Projekt DEAL.

**Open Access** Dieser Artikel wird unter der Creative Commons Namensnennung 4.0 International Lizenz veröffentlicht, welche die Nutzung, Vervielfältigung, Bearbeitung, Verbreitung und Wiedergabe in jeglichem Medium und Format erlaubt, sofern Sie den/die ursprünglichen Autor(en) und die Quelle ordnungsgemäß nennen, einen Link zur Creative Commons Lizenz beifügen und angeben, ob Änderungen vorgenommen wurden. Die in diesem Artikel enthaltenen Bilder und sonstiges Drittmaterial unterliegen ebenfalls der genannten Creative Commons Lizenz, sofern sich aus der Abbildungslegende nichts anderes ergibt. Sofern das betreffende Material nicht unter der genannten Creative Commons Lizenz steht und die betreffende Handlung nicht nach gesetzlichen Vorschriften erlaubt ist, ist für die oben aufgeführten Weiterverwendungen des Materials die Einwilligung des jeweiligen Rechteinhabers einzuholen. Weitere Details zur Lizenz entnehmen Sie bitte der Lizenzinformation auf http://creativecommons.org/licenses/by/4.0/deed.de.

## 7 Appendix

Table 1 Overview of studied electric vehicle traction motors and their associated characteristics [16]

| Supplier | Model | Model year | Vehicle dass | Motor-position | Motor topol-ogy | Power | | |
|---|---|---|---|---|---|---|---|---|
| | | | | | | Cont. [kW] | Peak [kW] | Faktor [-] |
| Hyundai | Kona electric Executive | 2018 | B | Front | PMSM | 28 | 150 | 5.36 |
| Jaguar | I-Pace EV 400 First Edition | 2018 | D | Front | PMSM | 90 | 147 | 1.63 |
| | | | | Rear | PMSM | 90 | 147 | 1.63 |
| Nissan | Leaf Tekna | 2018 | C | Front | EESM | 90 | 110 | 1.22 |
| Audi | e-tron 55 Quattro Edition One | 2019 | E | Front | IM | 70 | 135 | 1.93 |
| | | | | Rear | IM | 95 | 165 | 1.74 |
| Mercedes | EQC 400 4MAT1C 1886 Edition | 2019 | D | Front | IM | – | – | – |
| | | | | Rear | IM | 80 | 140 | 1.75 |
| Renault | Zoe RI35 Edition One | 2019 | B | Front | EESM | 51 | 100 | 1.96 |
| Aiways | U5 Premium | 2020 | D | Front | PMSM | 60 | 150 | 2.5 |
| Honda | E Advance | 2020 | B | Rear | PMSM | 60 | 113 | 1.88 |
| Peugeot | 208 e GT | 2020 | B | Front | EESM | 57 | 100 | 1.75 |
| Polestar | Long Range Dual Motor | 2020 | D | Front | PMSM | 80 | 150 | 1.88 |
| | | | | Rear | PMSM | 80 | 150 | 1.88 |
| VW | ID 3 Ist Max | 2020 | C | Rear | PMSM | 70 | 150 | 2.14 |
| Fiat | 500 e La Prima | 2020 | A | Front | PMSM | 43 | 87 | 2.02 |
| Hyundai | Ioniq 5 Project 45 | 2021 | C | Front | PMSM | – | 70 | – |
| | | | | Rear | PMSM | 53 | 155 | 2.92 |
| Mercedes | EQA 250 AMG Line | 2021 | C | Front | IM | 80 | 140 | 1.75 |
| Mercedes | EQS 580 4MATIC AMG Line | 2021 | F | Front | PMSM | 109 | 245 | 2.25 |
| | | | | Rear | PMSM | – | 140 | – |
| BMW | iX xDrive50 Sport | 2021 | E | Front | EESM | – | 190 | – |
| | | | | Rear | EESM | – | 230 | – |
| BYD | Tang EV | 2022 | D | Front | PMSM | – | 180 | – |
| | | | | Rear | PMSM | – | 200 | – |
| MG | 4 Mulan Luxury | 2022 | C | Rear | PMSM | 68 | 150 | 2.2 |
| Renault | Megane E-Tech Iconic EV60 | 2022 | C | Front | EESM | 55 | 160 | 2.9 |
| Tesla | Model YAWD Standard Range | 2022 | D | Front | IM | 65 | 158 | 2.43 |
| | | | | Rear | PMSM | 88 | 208 | 2.2 |
| BMW | i7 xDriveöO Individual | 2022 | F | Front | EESM | – | 190 | – |
| | | | | Rear | EESM | – | 230 | – |
| BMW | iX 1 xDrive30 Premium | 2022 | C | Front | EESM | – | 140 | – |
| | | | | Rear | EESM | – | 140 | – |
| Toyota | bZ4X | 2022 | C | Front | PMSM | 59 | 80 | 1.36 |
| | | | | Rear | PMSM | 59 | 80 | 1.36 |
| BYD | Seal Excellence | 2023 | D | Front | IM | 75 | 160 | 2.13 |
| | | | | Rear | PMSM | – | 230 | – |
| NIO | ET5 Long Range | 2023 | D | Front | IM | 30 | 150 | 5 |
| | | | | Rear | PMSM | 70 | 210 | 3 |
| Nissan | Ariya Evolve | 2023 | C | Front | EESM | 45 | 178 | 3.96 |
| Smart | #1 | 2023 | C | Rear | PMSM | 75 | 200 | 2.67 |
| Tesla | Model Y Standard Range | 2023 | D | Rear | PMSM | 90 | 235 | 2.61 |
| Polestar | 2 Long Range Dual Motor | 2023 | D | Front | IM | – | 110 | – |
| | | | | Rear | PMSM | 133 | 200 | 1.5 |
| Fisker | Ocean One | 2023 | D | Front | PMSM | – | – | – |
| | | | | Rear | PMSM | – | – | – |
| Volvo | EX30 Twin Motor | 2023 | C | Front | PMSM | – | 115 | – |
| | | | | Rear | PMSM | 75 | 200 | 2.67 |

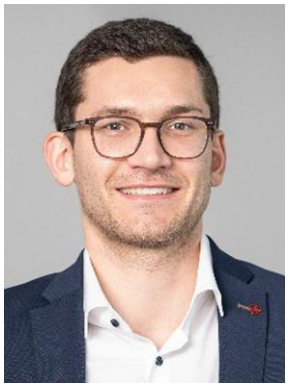
## References


1. Stampatori D, Raimondi PP, Noussan M (2020) Li-ion batteries: a review of a key technology for transport decarbonization. Energies 13(10):2638. https://doi.org/10.3390/en13102638
2. de Blas I, Mediavilla M, Capellán-Pérez I, Duce C (2020) The limits of transport decarbonization under the current growth paradigm. Energy Strategy Rev 32:100543. https://doi.org/10.1016/j.esr.2020.100543
3. Husain I et al (2021) Electric drive technology trends, challenges, and opportunities for future electric vehicles. Proc IEEE 109(6):1039–1059. https://doi.org/10.1109/JPROC.2020.3046112
4. Agamloh E, von Jouanne A, Yokochi A (2020) An overview of electric machine trends in modern electric vehicles. Machines 8(2):20. https://doi.org/10.3390/machines8020020
5. Rani S, Jayapragash R (2024) Review on electric mobility: trends, challenges and opportunities. Results Eng 23:102631. https://doi.org/10.1016/j.rineng.2024.102631
6. Asif M (2015) Determining improvement needs in higher education benchmarking. Benchmarking 22(1):56–74. https://doi.org/10.1108/BIJ-02-2013-0025
7. El Hadraoui H, Zegrari M, Chebak A, Laayati O, Guennouni N (2022) A multi-criteria analysis and trends of electric motors for electric vehicles. World Electr Veh J 13(4):65. https://doi.org/10.3390/wevj13040065
8. Oktav A (2011) New trends and recent development in automotive engineering. In: Chiaberge M (ed) New trends and developments in automotive system engineering. IntechOpen, Rijeka https://doi.org/10.5772/552
9. Wrobel R (2022) A technology overview of thermal management of integrated motor drives – electrical machines. Therm Sci Eng Prog 29:101222. https://doi.org/10.1016/j.tsep.2022.101222
10. Gai Y et al (2019) Cooling of automotive traction motors: schemes, examples, and computation methods. IEEE Trans Ind Electron 66(3):1681–1692. https://doi.org/10.1109/TIE.2018.2835397
11. Krings A, Monissen C (2020) Review and trends in electric traction motors for battery electric and hybrid vehicles. 2020 International Conference on Electrical Machines (ICEM), pp 1807–1813 https://doi.org/10.1109/ICEM49940.2020.9270946
12. International Energy Agency (IEA) (2024) Global EV outlook 2024: moving towards increased affordability. https://www.iea.org/reports/global-ev-outlook-2024. Accessed 26 Oct 2024
13. Cai W, Wu X, Zhou M, Liang Y, Wang Y (2021) Review and development of electric motor systems and electric powertrains for new energy vehicles. Automot Innov 4(1):3–22. https://doi.org/10.1007/s42154-021-00139-z
14. Khaleel M, Ahmed AA, Alsharif A, Beiek MM (2023) Technology challenges and trends of electric motor and drive in electric vehicle. Int J Electr Eng Sustain 1(1):41–48 (https://ijees.org/index.php/ijees/article/view/14)
15. A2MAC1 Database. https://www.a2mac1.com/
16. Allgemeiner Deutscher Automobil-Club e. V. (ADAC) Database "Automarken & Modelle". https://www.adac.de/rund-ums-fahrzeug/autokatalog/marken-modelle/?sort=SORTING_DESC
17. RWTH Aachen Production engineering of e-mobility components – tear-down studies. https://www.pem.rwth-aachen.de/go/id/fecr/
18. Commission of the European Communities (1999) Regulation (EEC) No 1064/89 Merger Procedure (Case No IV/M.1572 – ISS/Abilis)
19. Schäfer T (2016) Methodenlehre und Statistik: Einführung in Datenerhebung, deskriptive Statistik und Inferenzstatistik. Springer, Wiesbaden
20. Matsumori H (2022) Electrical and mechanical technology from the perspective of EV drive system, e-axle. J Japan Soc Appl Electromagn Mech 30(1):33–38. https://doi.org/10.14243/jsaem.30.33
21. Shimizu O et al (2022) Technical trend of next-generation application specific electric motors. International Power Electronics Conference (IPEC-Himeji 2022-ECCE Asia), pp 1978–1982 https://doi.org/10.23919/IPEC-Himeji2022-ECCE53331.2022.9807055
22. Ziegler M, Schäfer P, Wieprecht N, Franke J, Kühl A (2023) Investigation of insulation layers on additive manufactured electrical steel laminations in electric motors. IEEE Trans Dielectr Electr Insul 30(5):2344–2352. https://doi.org/10.1109/TDEI.2023.3261821
23. Ziegler M, Brandl F, Kuehl A, Franke J (2021) Evaluation of laser-welded electrical steel laminations for electric motors. 12th International Symposium on Advanced Topics in Electrical Engineering (ATEE), pp 1–6 https://doi.org/10.1109/ATEE52255.2021.9425168
24. Leuning N, Steentjes S, Hameyer K, Gerhards B, Reisgen U (2017) Analysis of a novel laser welding strategy for electrical steel laminations. 7th International Electric Drives Production Conference (EDPC), pp 1–8 https://doi.org/10.1109/EDPC.2017.8328144
25. Xia C, Wang H, Wu Y, Wang H (2020) Joining of the laminated electrical steels in motor manufacturing: a review. Materials (Basel) 13(20):4583. https://doi.org/10.3390/ma13204583
26. Krings A (2014) Iron losses in electrical machines: influence of material properties, manufacturing processes, and inverter operation. Dissertation, KTH School of Electrical Engineering
27. Zhang J, Spath D, He Y, Boronka A (2018) Cost-efficient selection of stamping machines for lamination production in the electric traction motor application. 8th International Electric Drives Production Conference (EDPC), pp 1–8 https://doi.org/10.1109/EDPC.2018.8658286
28. Finken T, Hombitzer M, Hameyer K (2010) Study and comparison of several permanent-magnet excited rotor types regarding their applicability in electric vehicles. 2010 Emobility – Electrical Power Train, Leipzig, 8–9 Nov 2010, pp 1–7 https://doi.org/10.1109/EMOBILITY.2010.5668074
29. Boglietti A, Cavagnino A, Lazzari M, Miotto A, Vaschetto S (2011) Induction motor design methodology based on rotor diameter progressive growth. 2011 IEEE Energy Conversion Congress and Exposition, pp 3104–3111 https://doi.org/10.1109/ECCE.2011.6064187
30. Bone J (1978) Influence of rotor diameter and length on the rating of induction motors. IEE J Electr Power Appl 1(1):2–6. https://doi.org/10.1049/ij-epa.1978.0002
31. Alberti L, Troncon D (2021) Design of electric motors and power drive systems according to efficiency standards. IEEE Trans Ind Electron 68(10):9287–9296. https://doi.org/10.1109/TIE.2020.3020028
32. Bach M, Babl A, Gerling D (2020) Integration of forming manufacturing technology into the component production of innovative electric motor concepts. 10th International Electric Drives Production Conference (EDPC), pp 1–8 https://doi.org/10.1109/EDPC51184.2020.9388210
33. Hagedorn J, Sell-Le Blanc F, Fleischer J (2018) Handbook of coil winding. Springer, Berlin https://doi.org/10.1007/978-3-662-54402-0
34. Halwas M, Hausmann L, Wirth F, Fleischer J, Jux B, Doppelbauer M (2020) Influences of design and manufacturing on the performance of electric traction drives.

2020 International Conference on Electrical Machines (ICEM), pp 488–494 https://doi.org/10.1109/ICEM49940.2020.9270899
35. Masoumi M, Rajasekhara K, Parati D, Bilgin B (2022) Manufacturing techniques for electric motor coils with round copper wires. IEEE Access 10:130212–130223. https://doi.org/10.1109/ACCESS.2022.3229024
36. Fleischer J, Haag S, Hofmann J (2017) Quo vadis Wickeltechnik? Eine Studie zum aktuellen Stand der Technik und zur Recherche zukünftiger Trends im Automobilbau. https://www.wbk.kit.edu/downloads/2017_02_21_Studie_Wickeltechnik_final_DE.pdf. Accessed 19 Apr 2025 (Institut für Produktionstechnik (wbk))
37. Yan Y, Mao C, Li C, Ren H (2024) Analysis and optimization of the winding loss of flat-wire motors. Electronics 13(16):3115. https://doi.org/10.3390/electronics13163115
38. Fang H, Chen Q, Wan X, Li A (2023) Design and optimization of high efficiency flat wire motor for electric vehicle. 2023 China Automation Congress (CAC), pp 4102–4107 https://doi.org/10.1109/CAC59555.2023.10451410
39. Di Leonardo L, Fabri G, Credo A, Tursini M, Villani M (2022) Impact of wire selection on the performance of an induction motor for automotive applications. Energies 15(11):3876. https://doi.org/10.3390/en15113876
40. Popescu M, Goss J, Staton DA, Hawkins D, Chong YC, Boglietti A (2018) Electrical vehicles – practical solutions for power traction motor systems. IEEE Trans Ind Appl 54(3):2751–2762. https://doi.org/10.1109/TIA.2018.2792459
41. Kampker A, Heimes HH, Dorn B, Brans F, Stäck C (2023) Challenges of the continuous hairpin technology for production techniques. Energy Rep 9:107–114. https://doi.org/10.1016/j.egyr.2022.10.370
42. Riedel A et al (2018) Challenges of the hairpin technology for production techniques. 21st International Conference on Electrical Machines and Systems (ICEMS), pp 2471–2476 https://doi.org/10.23919/ICEMS.2018.8549105
43. Kampker A, Heimes HH, Born H, Nankemann M, Backes T (2024) Production process of a hairpin stator. https://www.pem.rwth-aachen.de/global/show_document.asp?id=aaaaaaaacqfvmcd. Accessed 7 May 2025 (PEM of RWTH Aachen University)
44. Zhao Y, Li D, Pei T, Qu R (2019) Overview of the rectangular wire windings AC electrical machine. Trans Electr Mach Syst 3(2):160–169. https://doi.org/10.30941/CESTEMS.2019.00022
45. Kuehl A (2023) Optimized cutting process of flat wires for electric motors with hairpin technology. 2023 IEEE International Electric Machines & Drives Conference (IEMDC), pp 1–7 https://doi.org/10.1109/IEMDC55163.2023.10238786
46. Shenzhen HONEST Intelligent Equipments Co., Ltd. (2023) X-Pin motor performance and process feature. https://en.cnhonest.com/news/26.html. Accessed 24 Apr 2025
47. Sell-Le Blanc F (2025) Innovative ways to produce windings for e-machines that deliver higher performance and lower CAPEX. 12th Advanced E-Motor Technologies 2025, Munich, 27 Mar 2025
48. Dimier T, Cossale M, Wellerdieck T (2020) Comparison of stator winding technologies for high-speed motors in electric propulsion systems. 2020 International Conference on Electrical Machines (ICEM), pp 2406–2412 https://doi.org/10.1109/ICEM49940.2020.9270943
49. Born HC et al (2022) Manufacturing process and design requirements of litz wire with focus on efficiency improvement of traction motors. 12th International Electric Drives Production Conference (EDPC), pp 1–7 https://doi.org/10.1109/EDPC56367.2022.10019744
50. Zeynalova S, Cepparrone E, Roffino E, Barbero D (2024) Effect of thermal aging on electrical performance of perfluoroalkoxy- and polyamide-imide-coated magnet wire. IEE Electr Insul Mag 40(3):6–14. https://doi.org/10.1109/MEI.2024.10508410
51. Cavallini A (2024) High power density motors for transport electrification: state-of-the-art and challenges. 10th International Conference on Condition Monitoring and Diagnosis (CMD), pp 238–241 https://doi.org/10.23919/CMD62064.2024.10766263
52. Kampker A, Heimes HH, Dorn BN, Brans F, Born HC (2023) Application-oriented method for determining the adhesion between insulated flat copper wire and impregnation resin. In: Proceedings of the Conference on Production Systems and Logistics: CPSL 2023 – 1. publish-Ing., Hannover https://doi.org/10.15488/13494
53. Wirth F, Hausmann L, Fleischer J (2024) Model-based closed-loop process control for the manufacturing of hairpin coils. Prod Eng Res Devel 18:875–888. https://doi.org/10.1007/s11740-024-01271-5
54. Pushev G, Velev S, Dulgerov N (2016) Advanced conductor shape technology. Mach Technol Mater 10(12):3–7 (https://stumejournals.com/journals/mtm/2016/12/3)
55. Dix M, Bach M, Kräusel V, Wertheim R (2025) Efficient and sustainable production of electrical machines—achieving a higher slot fill factor through an innovative forming process chain. In: Kohl H, Seliger G, Dietrich F, Mur S (eds) Sustainable manufacturing as a driver for growth (GCSM 2023). Lecture Notes in Mechanical Engineering. Springer, Cham, pp 211–219 https://doi.org/10.1007/978-3-031-77429-4_24
56. Bonakdarpour M, Bailey TM (2022) The future of copper: Will the looming supply gap short-circuit the energy transition? https://cdn.ihsmarkit.com/www/pdf/0722/The-Future-of-Copper_Full-Report_14July2022.pdf. Accessed 20 Apr 2025
57. Eloot K et al (2024) Global materials perspective 2024. https://www.mckinsey.com/~/media/mckinsey/industries/energy%20and%20materials/our%20insights/global%20materials%20perspective%202024/global-materials-perspective-2024.pdf?shouldIndex=false. Accessed 7 May 2025
58. Farrell S, Whitton L (2024) BHP insights: How copper will shape our future. https://www.bhp.com/-/media/project/bhp1ip/bhp-com-en/documents/news/2024/240930_bhpinsights_howcopperwillshapeourfuture.pdf. Accessed 20 Apr 2025
59. IEA Publications (2021) Total copper demand by sector and scenario, 2020–2040. https://www.iea.org/data-and-statistics/charts/total-copper-demand-by-sector-and-scenario-2020-2040. Accessed 20 Apr 2025
60. Wrobel R, Williamson SJ, Booker JD, Mellor PH (2015) Characterising the performance of selected electrical machine insulation systems. 2015 IEEE Energy Conversion Congress and Exposition (ECCE), pp 4857–4864 https://doi.org/10.1109/ECCE.2015.7310345
61. Wrobel R, Williamson SJ, Booker JD, Mellor PH (2016) Characterizing the in situ thermal behavior of selected electrical machine insulation and impregnation materials. IEEE Trans Ind Appl 52(6):4678–4687. https://doi.org/10.1109/TIA.2016.2589219
62. Mayer D, Hausmann L, Maul N, Reinschmidt L, Hofmann J, Fleischer J (2019) Systematic investigation of the grooving process and its influence on slot insulation of stators with hairpin technology. 9th International Electric Drives

Production Conference (EDPC), pp 1–7 https://doi.org/10.1109/EDPC48408.2019.9011935
63. Calabrese E et al (2023) Thermal and electrical characterization of polyester resins suitable for electric motor insulation. Polymers 15(6):1374. https://doi.org/10.3390/polym15061374
64. Chapman M, Frost N, Bruetsch R (2008) Insulation systems for rotating low-voltage machines. Conference Record of the 2008 IEEE International Symposium on Electrical Insulation, pp 257–260 https://doi.org/10.1109/ELINSL.2008.4570323
65. Kampker A, Heimes HH (2024) Elektromobilität. Springer, Berlin https://doi.org/10.1007/978-3-662-65812-3
66. Kampker A et al (2024) Investigation of adhesion properties between secondary insulation and taped profiled high frequency litz wires. 14th International Electric Drives Production Conference (EDPC), pp 1–8 https://doi.org/10.1109/EDPC63771.2024.10932812
67. Born H, Drexler D (2025) Production and process innovations for continuous hairpin stators
68. Hassan W, Hussain GA, Mahmood F, Shafiq M, Montanari GC (2023) Effects of temperature and pressure on failure risk of electric motors based on partial discharge measurements. IEEE Trans Aerosp Electron Syst 59(5):5624–5633. https://doi.org/10.1109/TAES.2023.3262622
69. Baranski M, Szelag W, Lyskawinski W (2021) Experimental and simulation studies of partial demagnetization process of permanent magnets in electric motors. IEEE Trans Energy Convers 36(4):3137–3145. https://doi.org/10.1109/TEC.2021.3082903
70. Konovalov D et al (2023) Recent developments in cooling systems and cooling management for electric motors. Energies 16(19):7006. https://doi.org/10.3390/en16197006
71. Wang Q, Wu Y, Niu S, Zhao X (2022) Advances in thermal management technologies of electrical machines. Energies 15(9):3249. https://doi.org/10.3390/en15093249
72. Reinecke M et al (2024) Investigation of stator cooling concepts of an electric machine for maximization of continuous power. SAE Int J Adv Curr Pract Mobil 7(3):1187–1206. https://doi.org/10.4271/2024-01-3014
73. Huang J et al (2019) A hybrid electric vehicle motor cooling system—design, model, and control. IEEE Trans Veh Technol 68(5):4467–4478. https://doi.org/10.1109/TVT.2019.2902135
74. Shams Ghahfarokhi P, Podgornovs A, Kallaste A, Marques Cardoso AJ, Belahcen A, Vaimann T (2023) The oil spray cooling system of automotive traction motors: the state of the art. IEEE Trans Transp Electrif 9(1):428–451. https://doi.org/10.1109/TTE.2022.3189596
75. Gronwald P-O, Kern TA (2021) Traction motor cooling systems: a literature review and comparative study. IEEE Trans Transp Electrif 7(4):2892–2913. https://doi.org/10.1109/TTE.2021.3075844
76. Darius Gnanaraj S, Gundabattini E, Raja Singh R (2020) Materials for lightweight electric motors—a review. IOP Conf Ser Mater Sci Eng 906(1):12020. https://doi.org/10.1088/1757-899X/906/1/012020
77. AUDI AG (2024) Sporty performance: powerful drives. https://www.audi-mediacenter.com/en/the-audi-q6-e-tron-electric-mobility-on-a-new-level-15929/sporty-performance-powerful-drives-15932?utm.com#media-contacts. Accessed 7 May 2025
78. Eckhardt H (2021) Mission R: innovative e-motors, high-end battery and 900 volts. https://newsroom.porsche.com/en/2021/motorsports/porsche-concept-study-motorsports-mission-r-all-electric-gt-racing-car-drive-world-premiere-iaa-mobility-25603.html?utm.com. Accessed 21 Apr 2025
79. Fokker P (2023) Oog voor Techniek: VW APP550 is allround elektro-aandrijfpakket. https://www.amt.nl/76264/oog-voor-techniek-vw-app550-is-allround-elektro-aandrijfpakket. Accessed 7 May 2025 (in Dutch)
80. Procházka D (2024) Development of MEB drives – APP550: new e-drive of the ID. family. Konferenz zum elektrischen Antriebsstrang im Fahrzeug, Lindau, 16 Oct 2024
81. Lee T-Y, Song J-Y, Kim J, Kim Y-J, Jung S-Y, Je J-M (2014) Phase advance control to reduce torque ripple of brush-less DC motor according to winding connection, wye and delta. J Electr Eng Technol 9(6):2201–2208. https://doi.org/10.5370/JEET.2014.9.6.2201
82. Carney D (2024) Deep dive into Kia's innovative dual-wye-and-delta EV motor configurations. https://www.designnews.com/automotive-engineering/deep-dive-into-kia-s-innovative-dual-wye-and-delta-ev-motor-configurations. Accessed 22 Apr 2025
83. Dlala E (2024) Electric motor with permanent magnets abutted by tabs in lamination cavities (Patent US11909270B2, 1 June 2021)
84. Dai Y, Lee H-J (2024) Torque ripple and electromagnetic vibration suppression of fractional slot distributed winding ISG motors by rotor notching and skewing. Energies 17(19):4964. https://doi.org/10.3390/en17194964
85. Yan D, Yan Y, Cheng Y, Guo L, Shi T (2024) Research on cogging torque reduction method for permanent magnet synchronous motor accounting for the magnetic pole edge effect. IET Electr Power Appl 18(1):64–75. https://doi.org/10.1049/elp2.12367
86. Blum J, Merwerth J, Herzog H-G (2014) Investigation of the segment order in step-skewed synchronous machines on noise and vibration. 4th International Electric Drives Production Conference (EDPC), pp 1–6 https://doi.org/10.1109/EDPC.2014.6984413
87. Rosen A, Weicherding Z, Hellenbroich G et al (2025) Elektrische Antriebseinheit mit Doppelrotor-Radialflussmotor und SiC-Wechselrichter. MTZ Motortech Z 86(5):28–35. https://doi.org/10.1007/s35146-025-2067-y

**Publisher's Note** Springer Nature remains neutral with regard to jurisdictional claims in published maps and institutional affiliations.



**David Drexler,** born in Lüneburg in 1996, received his Bachelor and Master of Science in Business Administration and Engineering: Mechanical Engineering Production Technology from RWTH Aachen University in 2021 and 2023 respectively. He also received an additional Master of Science in Automotive Engineering from Tsinghua University in 2024. In 2024 he started as a research associate at the Institute for Production Engineering of E-Mobility Components (PEM) of RWTH Aachen University. His research focuses on production processes for Litz wire as an alternative conductor topology for high-frequency electric traction applications.



**Achim Kampker,** Professor, studied mechanical engineering with a focus on production engineering and is the founder as well as the director of the Chair of Production Engineering of E-Mobility Components (PEM) of RWTH Aachen University, Germany. In numerous research groups, he and his team are dedicated to the production, development, and recycling of battery systems and their components as well as hydrogen technologies, the electric powertrain, and entire vehicle concepts such as electric heavy-duty trucks. Kampker, who in addition to his expertise in electric mobility components and concepts in teaching and research also has many years of experience in the management of start-ups and established companies, co-developed the electric "Streetscooter" vehicle in Aachen and was CEO of StreetScooter GmbH from December 2014 to April 2019. In addition to teaching at RWTH Aachen University, Kampker serves as a member of the institute management of the Fraunhofer Research Institution for Battery Cell Production FFB in Münster, Germany



**Henrik Born,** born in 1994, received his Bachelor's and Master's degree in Mechanical Engineering and Business Administration from the RWTH Aachen University in 2017 and 2019. In 2020 he started his academic career at the Chair of Production Engineering of E-Mobility Components (PEM) of RWTH Aachen University in the field of electric drive production. The main focus as research assistant was on product and process development for the efficient production of hairpin stators. Since 2024, he leads the research areas of battery production and electric motor production as head of department of the same institute.



**Michael Nankemann,** received his Bachelor and Master of Science in Business Administration and Engineering: Mechanical Engineering Production Technology from RWTH Aachen University in 2018 and 2020 respectively. In 2021 he started as research associate at the Institute for Production Engineering of E-Mobility Components. Since 2024 he is responsible for the research group Electric Drive Production as group lead. His research is focused on sustainability assessments in early stages of technology development.



**Sebastian Hartmann,** was born in Tübingen in 1991. He received his Bachelor of Engineering in Mechanical Engineering from Esslingen University of Applied Sciences in 2015 and afterwards the Master of Science in Mechanical Engineering from Reutlingen University of Applied Sciences in 2017, specializing in Design & Development and Product Development respectively. Since 2022, he has been with the Chair of Production Engineering of E-Mobility Components (PEM) at RWTH Aachen University as a Ph.D. candidate in the field of Electric Drive Production.



**Tobias Kulawik,** was born in 1989 in Düsseldorf. Until 2022 he worked as an Area Manager at Domino's Pizza and received on his way back to his passion for technology a Bachelor of Science in Mechanical Engineering from RWTH Aachen University in 2023. He is currently pursuing his Master's degree in Mechanical Engineering at RWTH Aachen University.